RHESSys: Regional Hydro-Ecologic Simulation System—An Object-Oriented Approach to Spatially Distributed Modeling of Carbon, Water, and Nutrient Cycling

C.L. Tague*

Department of Geography, San Diego State University, San Diego, California

L.E. Band

Department of Geography, University of North Carolina at Chapel Hill, Chapel Hill, North Carolina

Received 29 October 2003; accepted 3 February 2004

ABSTRACT: Process-based models that can represent multiple and interacting processes provide a framework for combining field-based measurements with evolving science-based models of specific hydroecological processes. Use of these models, however, requires that the representation of processes and key assumptions involved be understood by the user community. This paper provides a full description of process implementation in the most recent version of the Regional Hydro-Ecological Simulation System (RHESSys), a model that has been applied in a wide variety of research

* Corresponding author address: C.L. Tague, Department of Geography, San Diego State University, 5500 Campanile Drive, San Diego, CA 92182-4493.
E-mail address: ctague@mail.sdsu.edu

settings. An overview of the underlying (Geographic Information System) GIS-based model framework is given followed by a description of the mathematical models used to represent various biogeochemical cycling and hydrologic processes including vertical and lateral hydrologic fluxes, microclimate variability, canopy radiation transfer, vegetation and soil microbial carbon and nitrogen cycling. An example application of RHESSys for a small forested watershed as part of the Baltimore Long-Term Ecological Research site is included to illustrate use of the model in exploring spatial-temporal dynamics and the coupling between hydrology and biogeochemical cycling.

KEYWORDS: Hydrology, Modeling, Ecosystems

1. Introduction

The Regional Hydro-Ecological Simulation System (RHESSys) is a hydro-ecological model designed to simulate integrated water, carbon, and nutrient cycling and transport over spatially variable terrain at small (first-order streams) to medium (fourth- and fifth-order streams) scales. The model is structured as a spatially nested hierarchical representation of the landscape with a range of hydrological, microclimate, and ecosystem processes associated with specific landscape objects at different levels of the hierarchy. This approach is designed to facilitate environmental analysis that requires an understanding of within-watershed processes as well as aggregate fluxes of water, carbon, and nitrogen.

As a hydrologic model, RHESSys is intermediate in terms of complexity. Unlike lumped parameter hydrologic models such as the Identification of unit Hydrographs and Component flows from Rainfall, Evaporation, and Streamflow data (IHACRES; Evans and Jakeman 1998) or empirical curve number approaches, RHESSys explicitly models connectivity and lateral hydrologic fluxes between landscape units within a watershed. The representation of the vertical soil profile, however, is based on a fairly simple two-layer model with a single unsaturated and saturated zone. Additional hydrologic stores include a litter layer, surface detention store, multiple canopy interception layers, and a snowpack. Process-based hydrologic models such as MIKE-SHE (Refsgaard and Storm 1995) are at the more complex end of the continuum and provide a 1D Richard's equation solution to drainage through multiple soil layers down to the saturated zone. In addition to hydrology, RHESSys is able to model feedbacks between hydrology and ecosystem carbon and nutrient cycling, including the growth of vegetation. Other process-based eco-hydrologic models such as Macaque (Watson et al. 1999) and Topog (Vertessy et al. 1993) also provide this capability. In each of these models, representation of specific processes may differ but these models are relatively similar in terms of overall complexity.

The version of RHESSys described in this paper has evolved from the integration of stand-level ecosystem models with methods to compute the distribution and flux of soil water at the landscape level. These earlier versions of RHESSys were designed to explicitly couple the Forest Biogeochemical Cycles (FOREST-BGC) canopy model (Running and Coughlan 1988) with landscape-level patterns of critical meteorological forcing (Running et al. 1987) and later with hydrologic processes using the TOPMODEL (Beven and Kirkby 1979) hydrologic model. The first approach to distribute ecosystem processes at the landscape level

involved gridding the "topclimatic" logic of Mountain Climate Simulator (MTN-CLIM) with FOREST-BGC for a 1200 km^2 watershed in western Montana (Running et al. 1987). Later versions of RHESSys followed a generalization of FOREST-BGC to multiple biomes as Biome biogeochemical cycles Model (BIOME-BGC) (Running and Hunt 1993). Hydrologic modeling studies using RHESSys have included analysis of model sensitivity to landscape representation (Band 1993; Band et al. 1993) and using the model to explore the sensitivity of hydrologic response to climate change (Baron et al. 1998).

This current version of RHESSys continues to follow the basic BIOME-BGC framework. As discussed in this paper, however, many submodels used for specific processes have been altered and/or extended, largely to improve the soil biogeochemical process representation and expand canopy representation to consider both understory and overstory layers. Representation of soil organic matter decomposition in both RHESSys and BIOME-BGC is based largely on the CENTURY model. RHESSys also uses the $\text{CENTURY}_{\text{NGAS}}$ (Parton et al. 1996) approach to model (nitrogen) N-cycling processes such as nitrification and denitrification.

The current version of RHESSys has extended these hydrologic studies through the incorporation of an explicit hydrologic routing model in place of TOPMODEL. This current version has been used to explore the combined impact of roads and forest harvesting for several catchments in the Pacific Northwest (Tague and Band 2001; Krezek 2001), as well as in the Canadian boreal plain (Creed et al. 2000).

Coupled hydrologic-ecosystem and biogeochemical cycling studies using RHESSys include Mackay and Band (Mackay and Band 1997) who applied an earlier version of RHESSys to estimate carbon cycling in a small forested watershed. Mitchell and Csillag (Mitchell and Csillag 2000) are using the current version of RHESSys to explore spatially varying soil moisture controls on grassland productivity. Creed and Band (Creed and Band 1998) illustrate the use of similarity indices, derived using an earlier version of RHESSys, to compute a nitrate-flushing index based on saturation and a source index based on nitrate availability and dynamics in the saturation zone for a set of forested catchments in Ontario, Canada. By using these similarity indices, Creed and Band (Creed and Band 1998) were able to explain a significant amount of the variation in nitrate export between catchments and over time within the region. These indices, however, did not explicitly model N cycling and transport dynamics. Explicit modeling of N cycling and transport dynamics is included in the current version of RHESSys and has been tested for a small forested watershed as part of the Baltimore Ecosystem Study (BES; Band et al. 2001). The current version is also being used to explore spatial variation in N cycling in the Rocky Mountains (Laundrum et al. 2002), N saturation in the Smokey Mountains (Webster et al. 2001), and to examine the alteration of N sources and sinks along hydrologic flowpaths along a gradient of urbanization as part of the BES (Tague et al. 2000).

2. Implementation and model structure

One of the unique features of RHESSys is its hierarchical landscape representation. This approach allows different processes to be modeled at different scales and allows basic modeling units to be of arbitrary shape rather than strictly grid based.

RHESSys is also structured using an object-based design approach to facilitate algorithmic substitution. Additional details on model hierarchical structure and coding implementation can be found in Band et al. (Band et al. 2000).

RHESSys partitions the landscape such that each level of the spatial hierarchy fully covers the spatial extent of the landscape. Spatial levels define a containment hierarchy with progressively finer units. Each spatial level is associated with different processes modeled by RHESSys and with a particular scale. At the finest scale, patches are typically defined on the order of meters squared, while basins (km^2) define the largest scale.

Within RHESSys, a given spatial level is defined as a particular object type with a set of state (storage) and flux variables, process representations (equation sets), and an associated set of model parameters. For example, the estimation of atmospheric flux variables such as radiation occurs at the zone level. Thus, in deriving the set of spatial objects for a given simulation, zones are chosen to represent areas of similar climate or atmospheric-forcing conditions. The advantage of this hierarchical approach is that it allows different processes, that is, climate versus canopy processes, to be modeled at different spatial and temporal scales. It also allows modeling to occur on ecologically meaningful units as opposed to arbitrarily defined grid cells.

The definition of modeling units is done by the user prior to running the simulation. Although the user is given considerable flexibility in choosing a partitioning strategy for the different levels, partitioning should be tailored to take advantage of the patterns of relevant variability within the landscape and, in the case of patches, to maintain a coherent and solvable flow network. This permits efficient parameterization and reduces the error associated with landscape partitioning. Band et al. (Band et al. 1991), Lammers et al. (Lammers et al. 1997), and Tague et al. (Tague et al. 2000) provide further justification for and discussion of partitioning strategies, although this is an area requiring additional development.

2.1. Basins

Basins are defined as hydrologically closed drainage areas and encompass a single stream network. Basins typically serve as aggregating units to determine net fluxes of carbon, water, and nitrogen over the entire study area.

At present, RHESSys accounts for routing (storage and flux) of water within hillslopes to the stream. Once water reaches the stream, however, it is assumed to exit the basin within a single (daily) time step. For larger basins or shorter time steps, in-stream channel processes can be important. Future versions of RHESSys will likely use basins to organize the combination of hillslopes and stream reaches as separate object types and include a channel-routing model for stream reaches within the basin stream network.

2.2. Hillslopes

Hillslopes define areas that drain into one side of a single stream reach. Explicit routing between patches is organized at the hillslope level to produce streamflow. Hillslopes will usually be derived based upon drainage patterns using (Geographic Information System) GIS-based terrain-partitioning algorithms such as r.watershed

in GRASS (Geographic Resources Analysis Support System) GIS environment and as described in Lammers and Band (Lammers and Band 1990). Like basins, hillslopes can also be used to aggregate sublevel processes. The spatial redistribution of patch soil moisture is organized at the hillslope level and, for simulations that use TOPMODEL for lateral flow distribution, a hillslope-level base flow is defined.

2.3. Zones

Zones denote areas of similar climate. Zone objects contain meteorological variables and use topclimate extrapolation methods necessary to characterize spatial variation in these variables. Each zone is linked to a particular set of climate input files. Thus, a given landscape may use data from multiple meteorological stations or atmospheric model grid cells if this information is available. Data from a particular station are modified based on zone elevation, slope, and aspect relative to the input climate station. Zone processing also estimates additional climate variables that may not be available from base climate station information such as vapor pressure deficit. Numerous strategies exist to partition areas of similar climate. Elevation bands in a mountainous area, for example, are likely to denote areas of similar climate and exposure as discussed in Lammers et al. (Lammers et al. 1997). The distribution of climate stations can also be used to define zone partitioning, where each zone defines the area associated with a particular climate station.

2.4. Patches

Patches represent the smallest-resolution spatial unit and define areas of similar soil moisture and land-cover characteristics. Vertical soil moisture processing and soil biogeochemistry are modeled at the patch level. Patch variables include fluxes such as infiltration, saturation zone recharge, and soil nutrient cycling. Patches are often derived using an overlay of several different maps, such as a wetness index, vegetation cover, and stream and road network layers. Patch definition, however, must also be designed to maintain the underlying topographic controls on drainage patterns in the watershed. Patches can be defined that contain a stream channel and parameterized to regulate land-channel drainage flux. In landscapes modified by humans, patches may also be defined to contain a stream channel, road segments, or storm sewers that provide specific drainage conditions. Human sources of water and nutrients including irrigation, fertilization, and septic system input are also defined at this level.

2.5. Canopy strata

Canopy strata are a separate object type but they define vertical, aboveground layers rather than horizontal spatial layers. The spatial resolution of the canopy stratum is defined by the patch partitioning. Processes such as photosynthesis and transpiration are modeled at the canopy stratum level. Each stratum corresponds to a different layer such as overstory or understory in the canopy structure. The user defines the number of vertical layers. A height state variable is associated with each layer and defines its processing relative to the other layers. Incoming radiation,

precipitation throughfall, and wind are extinguished through the multiple layers according to the height and vegetation characteristics of each layer. RHESSys also permits multiple strata at the same height. This allows mixed vegetation types within the same spatial area to be represented. Finally, a litter layer is defined at the patch level and receives input from the overlying canopy layers. This litter layer acts as the interface between each patch and its associated canopy strata layers. For nonvegetated patches, a dummy litter layer (with no attenuation or processing of hydrologic, energy and carbon/nutrient fluxes) is used.

2.6. Interface

Parameterization and management of RHESSys is complex due to the multiple levels of spatial partitioning and the associated parameter sets. Most of these parameters are derived from topographic, land-cover, and soil map layers. Associated with RHESSys are a number of interface programs, which organize input data into the format required by the simulation model. These include standard GIS-based terrain-partitioning programs and RHESSys-specific programs that derive landscape representation from GIS images and establish connectivity between spatial units. These various programs can be run in stand-alone mode or as part of an integrated RHESSys interface, RAINMENT. Additional details about the RHESSys interface can be found in Band et al. (Band et al. 2000).

Key inputs into RHESSys include (see Figure 1) the following.

1. A description (worldfile) of the landscape representation and initial-state variables associated with each component of the spatial hierarchy (i.e., basins, hillslopes, zones, etc.) Because of the length and spatial complexity incorporated in this description, GRASS and ARCVIEW GIS-based programs (GRASS2WORLD, ARCVIEW2WORLD) were developed to generate this file.
2. The flow table describes connectivity between patches within a hillslope when the explicit routing approach is used to model distributed hydrology. The flow table is also generated automatically prior to running the main RHESSys simulation using a software program (CREATE-FLOWPATHS).
3. The temporal event control (TEC) file describes the timing and nature of temporal events that will occur during the course of the simulation, that is, disturbances such as forest harvesting, fire, or road construction. Temporal events refer to events that initiate a change in landscape-state variables or parameterization or new processes in the simulation sequence. A spinup period is typically run prior to output to remove transient behavior due to initialization.The TEC file is also used to control data assimilation for output.
4. Time series inputs include a range of climate variables as discussed in section 3, along with descriptions of the station at which this information was collected. Each zone in the spatial hierarchy is associated with a particular climate station. Note that base station coverage can be defined at any level of the hierarchy and need not be spatially contained by hillslopes, zones, or patches. Input stations can also be assigned at the patch level to organize fertilizer and irrigation inputs.
5. Parameter files are associated with each level of the spatial hierarchy. A

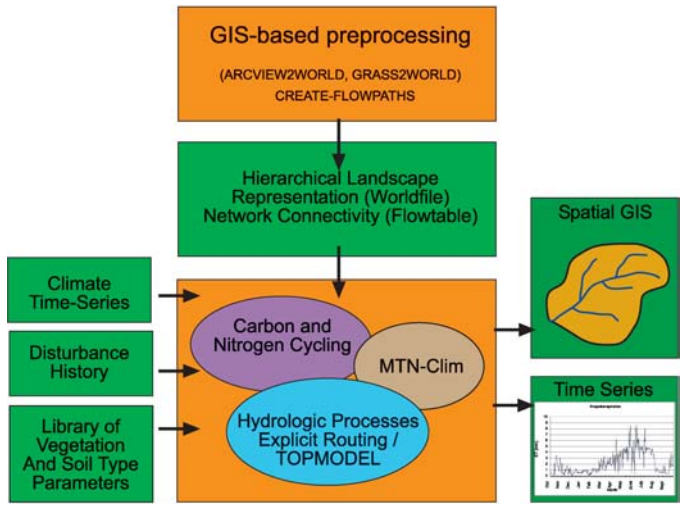

Figure 1. RHESSys model structure: Inputs, output, and preprocessing.

library of commonly used parameter files assigned to specific soil and vegetation types is available. The current library of parameter files include standard parameters for conifer, deciduous, grass, chaparral, tundra, as well as a number of more refined files for specific species groups such maple, pine, spruce, oak, aspen, or douglas fir. The current library of parameter files include all major soil textures, such as clay, sandy loam, etc.

2.7. Implementation and future development

This current version of RHESSys is implemented in the C programming language using an object-based approach to facilitate the substitution of different process algorithms. All of the processes as well as input/output routines are contained in separate procedures with appropriate names. This allows for relatively easy modification of specific process algorithms. Data structures are similarly defined and named to maintain clarity about the level of the spatial hierarchy associated with a specific algorithm.

The object-based approach and hierarchical landscape representation are also designed to facilitate future RHESSys development. Structures exist to allow for the development of subdaily time step models for certain processes such as infiltration. Object-based landscape representation also facilitates the implementation of different land covers such as those found in urban areas. Hillslope-level organization of drainage and particularly the implementation of roads as mechanisms by which flow can be redirected serve as a foundation for implementation of other man-made controls on flowpaths such as sewers.

3. Atmospheric and environmental forcing

Atmospheric variables or external forcing variables drive RHESSys hydrology and biogeochemical cycling. These include climate variables such as daily temperature

and precipitation as well as material inputs such as atmospheric nitrogen deposition. Climate input and processing in RHESSys is done at the zone level. Each zone is assigned a particular base station that manages external time series inputs to the model. Multiple zone objects can be assigned to the same base station; however, each zone must have a unique base station associated with it. The appendix lists current atmospheric variables that are used internally in the model. For most of these variables, the user has the option of providing a daily time series as input (associated with its base station) or allowing RHESSys to estimate the daily value from user parameters. Daily temperature and precipitation, however, must be input by the user. Input time series may be derived from field observation or from coupling with external models. Internal estimation of most meteorological variables, including incoming radiation, is based on algorithms from the MTN-CLIM model (Running et al. 1987).

Currently, nitrogen and precipitation are the only material inputs into the model. Atmospheric nitrogen deposition as nitrate and as ammonium are input as separate time series in RHESSys. Wet and dry deposition, however, are not distinguished in the current model. If a time series of nitrogen deposition is not provided, a constant daily value for nitrate based on a zone parameter will be used. In this case, deposition as ammonium is assumed to be zero.

3.1. Temperature

Daily minimum and maximum temperature time series must be included in the base station assigned to each zone object. Note that these time series may be derived from field observations or from an external mesoscale atmospheric model such as the Regional Atmospheric Modeling System (RAMS; Walko et al. 2000) or external climate interpolation schemes such as the Parameter-Elevation Regressions on Independent Slopes Model (PRISM; Daly et al. 1994) or Daymet (Thornton et al. 1997). For each zone, the base station temperatures are scaled by a lapse rate with elevation (included as a zone parameter).

Dewpoint temperature, if it is included with base station data, is similarly adjusted by a dewpoint lapse rate. If it is not input as a time series, it is assumed to be the minimum temperature value, after the elevation adjustment. Rooting zone soil temperature is computed as a running average of average air temperature similar to Zheng et al. (Zheng et al. 1993):

$$T_{\text{soil}}(t) = 0.9\left[T_{\text{soil}(t-1)}\right] + 0.1(T_{\text{avg}}), \tag{1}$$

where T_{soil} is rooting zone soil temperature and T_{avg} is average daily temperature. The buffering effect of snow cover is not taken into account.

3.2. Precipitation

A daily precipitation time series must also be included in each base station and can be adjusted using an isohyetal multiplier assigned to each zone. Orographic patterns in precipitation can be modeled using this isohyetal multiplier. Rainfall duration defaults to the entire day, unless a rainfall duration time series is included as a base station input. The user also has the option of providing hourly, rather than daily, rainfall input and running the hydrologic portion of the model in an hourly mode.

The user may input a snowfall time series directly. If a snowfall time series is not included, precipitation is partitioned into rain and snow by assuming a linear transition from snow to rain across a temperature range defined by $T_{\min_{rain}}$ and $T_{\max_{snow}}$, which are zone parameters indicating the minimum temperature at which rain can occur and the maximum temperature at which snow can occur, respectively.

3.3. Vapor pressure deficit

Saturation vapor pressure and relative humidity can be input directly. If these observations are not available from the base station climate file, saturation vapor pressure and vapor pressure deficit are estimated from standard air temperature–vapor pressure relationships (Jones 1992).

3.4. Incoming radiation

Canopy radiation interception (see section 5.2.) depends upon top of canopy inputs of both diffuse ($K_{diffuse'}$) and direct ($K_{direct'}$) solar radiation as well as longwave radiation. These radiation streams can be input by the user as part of the climate base station or can be estimated internally in the model. Within RHESSys, a solar geometric-based estimate of atmospheric radiation is computed based on site latitude, zone slope, aspect, and east–west horizon values. Incoming radiation is then adjusted to account for atmospheric transmissivity, estimated based on daily temperature variation and precipitation. These equations are not described here since they directly follow the MTN-CLIM approach (Running et al. 1987).

3.5. Atmospheric CO_2

In the current version of RHESSys, atmospheric CO_2 concentration is held constant at 370 ppm. (Note: CO_2 concentration is used in estimates of stomatal conductance.) It is included as a state variable, however, such that it can be readily modified in future versions.

4. Soil hydrologic processes and transport mechanisms

Vertical and lateral soil moisture and associated nutrient fluxes are modeled for each patch object. Patch topology (i.e., connectivity between patches) is organized by basin objects.

To model vertical soil moisture processes, a simple three-layer model is used, which includes a surface detention store, an unsaturated store, and a saturated store. Snowpack and litter stores are also included.

Water can also be stored in the vegetation and litter layers above each patch as interception storage (see section 5.5.). The soil column consists of two variable depth layers: an unsaturated zone and a saturated zone. The boundary between the saturated and unsaturated zone is defined by the saturation deficit (s as a water equivalent deficit and z as an actual depth to saturation). Vertical fluxes between each soil compartment are modeled to preserve mass balances such that, for each time step

$$\Delta s = -q_{\text{drain}} + q_{\text{cap}} + \text{ET}_{\text{sat}} \tag{2}$$

$$\Delta s_{\text{unsat}} = q_{\text{infil}} - q_{\text{drain}} + q_{\text{cap}} - \text{ET}_{\text{unsat}} \tag{3}$$

$$\Delta \text{det}S = \text{TF} + q_{\text{melt}} - q_{\text{infil}} - E, \tag{4}$$

where q_{drain}, q_{cap}, and q_{infil} are drainage from the unsaturated zone, capilliary rise, and infiltration, respectively; ET_{sat} and ET_{unsat} are evapotranspiration from the saturated and unsaturated zone, respectively; s_{unsat} is the soil moisture content of the unsatured zone and det$S$ is the surface detention storage; TF is the net throughfall from canopy layers; E is the surface storage evaporation; and q_{melt} is snowmelt. All stores are maintained as meters of water and fluxes as meters per day.

4.1. Detention storage and infiltration

At each time step, net throughfall from canopy layers and snowmelt are added to current surface detention storage and allowed to infiltrate into the soil following Phillip's infiltration equation (Phillip 1957):

$$q_{\text{infil}} = It_p + S_p\sqrt{t_d - t_p} + K_{\text{sat}_s}(t_d - t_p) \quad \text{for} \quad t_d > t_p,$$
$$q_{\text{infil}} = It_d \quad \text{for} \quad t_d < t_p, \tag{5}$$

where q_{infil} is infiltration; I and t_d are input intensity and duration; and K_{sat_s} is saturated hydraulic conductivity at the wetting front, defined by the saturation depth z. [Equation (8) is used to compute K_{sat_s} at depth z.] Estimation of sorptivity S_p is based on Manley (Manley 1977):

$$S_p = \sqrt{2}K_{\text{sat}_s}0.76\varphi_{\text{ae}}, \tag{6}$$

where φ_{ae} is air entry pressure, which is set as a soil specific input parameter.

Time to ponding is denoted as t_p, which is computed using the Green and Ampt approximations (Green and Ampt 1911) as follows:

$$t_p = K_{\text{sat}_s}0.76\varphi_{\text{ae}}\frac{(\phi - \theta_0)}{I(I - K_{\text{sat}_s})}, \tag{7}$$

where ϕ is porosity and θ_0 is initial soil moisture content.

If a daily time step is used, it is assumed that all inputs (precipitation and snowmelt) are distributed evenly throughout the day. In regions characterized by high-intensity, short-duration rainfall, this approach will overestimate infiltration rates. In these cases, the user may choose to input a rainfall duration time series, which will override the assumption of a daily duration.

Ponded water that is not infiltrated within the daily time step becomes detention storage. Detention storage beyond a surface detention storage capacity parameter will become overland flow.

4.2. Hydraulic conductivity and porosity profiles

The vertical hydraulic conductivity profile controls both vertical and lateral soil moisture fluxes in RHESSys. In the current implementation an exponential profile is the default; although alternative profiles may be substituted for specific field sites where the soil conductivity profile does not fit this exponential mode (e.g.,

Ambroise et al. 1996). Thus, saturated hydraulic conductivity, $K_{\text{sat}}(z)$ is computed as

$$K_{\text{sat}}(z) = K_{\text{sat}_0} \exp^{(-\frac{z}{m})}, \tag{8}$$

where K_{sat_0} is hydraulic conductivity at the surface and m describes the decay rate of conductivity with depth. Both are set as soil-type-specific input parameters. Hydraulic conductivity profiles are difficult to measure and may vary widely for a given soil texture/type. Further, field evidence suggests that at scales greater than centimeters, conductivity controls on hydrologic fluxes must consider both the properties of the soil matrix and macropore/preferential flowpath distributions (McDonnell 1990). To account for both uncertainty in conductivity profiles and preferential flow, both m and K_{sat_0} are typically calibrated against observed streamflow values in RHESSys (see section 7).

Porosity is also permitted to vary with depth such that

$$\phi(z) = \phi_0 \exp^{-\frac{z}{p}}, \tag{9}$$

where ϕ_0 and p are soil specific parameters defining surface porosity and the decay of porosity with depth, respectively. Setting a large value of p (e.g., $p > 1000.0$) allows a constant porosity to be assumed. Saturated soil moisture storage for a given profile section must be calculated by integrating porosity over the associated depth.

4.3. Vertical unsaturated zone drainage

As noted above, RHESSys maintains both an unsaturated and saturated zone. Drainage from the unsaturated zone to the saturated zone, q_{drain}, is limited by field capacity θ_{fc} of the unsaturated zone (computed by integrading a pressure gradient of -1 over the unsaturated profile), and by the vertical unsaturated hydraulic conductivity at the boundary $[K_{\text{unsat}}(z)]$ between the unsaturated and saturated zone such that

$$q_{\text{drain}} = \min[K_{\text{unsat}}(z_s)dT, \theta_{\text{unsat}} - \theta_{\text{fc}}], \tag{10}$$

where dT is the time step.

Here $K_{\text{unsat}}(z)$ can be estimated using either vanGenuchten and Nielsen (vanGenuchten and Nielsen 1984) or Clapp and Hornberger (Clapp and Hornberger 1978) models of soil characteristics.

In the Clapp and Hornberger (Clapp and Hornberger 1978) approach:

$$K_{\text{unsat}}(z) = K_{\text{sat}}(z)S^{(2b+3)}, \tag{11}$$

where b is the pore size index, a soil-specific parameter; $K_{\text{sat0}}(z)$ is calculated using Equation (8), and S is relative saturation.

If the vanGenuchten approach is used:

$$K_{\text{unsat}}(z) = K_{\text{sat0}}(z)S^{0.5}[1 - (1 - S^{\frac{1}{c}})^c]^2, \tag{12}$$

where c is a soil-specific parameter.

To compute a depth of unsaturated zone soil moisture at field capacity [θ_{fc} in Equation (10)], the relative saturation at field capacity is integrated over the porosity profile from the surface to the water table depth (z_s).

Relative saturation at field capacity S_{fc} is derived again based on either the Clapp

and Hornberger (Clapp and Hornberger 1978) or vanGenuchten and Nielsen (vanGenuchten and Nielsen 1984) assumptions such that, respectively,

$$S_{\mathrm{fc}}(z) = \left[\frac{\varphi_{\mathrm{ae}}}{(z_s - z)}\right]^b, \tag{13}$$

$$S_{\mathrm{fc}}(z) = \left[1 - \frac{(z_s - z)^{-b}}{\varphi_{\mathrm{ae}}^c}\right]. \tag{14}$$

Note that b and c are the soil-specific parameters used in Equations (11)–(12) above, φ_{ae} is the air entry pressure, again assigned based on soil type.

4.4. Soil evaporation

Soil evaporation is limited both by energy and atmospheric drivers and by a maximum exfiltration rate as a function of soil properties at a given soil moisture.

Soil moisture limits on soil evaporation are accounted for using a potential exfiltration rate, $\mathrm{pot}_{q_{\mathrm{exfil}}}$, based on a modification of Eagleson (Eagleson 1978) by Wigmosta et al. (Wigmosta et al. 1994) such that

$$\mathrm{pot}_{q_{\mathrm{exfil}}} = \left[S^{\frac{1}{2b}}\sqrt{\frac{8\bar{\phi}\bar{K}_{\mathrm{sat}}\varphi_{\mathrm{ae}}}{3(1+3b)(1+4b)}}\right], \tag{15}$$

where b is the pore size index. Porosity ($\bar{\phi}$) and saturated hydraulic conductivity ($\bar{K}_{\mathrm{sat}}$) are averaged over depth to saturation (z_s) using Equations (9) and (8), respectively, and S is the relative soil moisture content computed as (unsat/s) with an added restriction of a maximum active soil depth over which the exfiltration process applies. Thus, if the saturation deficit is greater than an active soil depth, the relative soil moisture S is computed as unsat/$s_{\mathrm{active.soil.depth}}$. Active soil depth is included as a soil-specific parameter.

Energy and atmospheric drivers of soil evaporation are accounted for using the Penman–Monteith equation (see section 5.6.). Surface conductance for soil is based on empirical relationships between rooting zone soil water content θ and diffusive resistance C_{surf}, as observed by Kelliher et al. (Kelliher et al. 1986) in a douglas fir forest:

$$\begin{aligned} C_{\mathrm{surf}} &= 0.001\ 429 \quad \text{for} \quad \theta > 0.185, \\ C_{\mathrm{surf}} &= \frac{1}{-83\ 000\theta + 16\ 100} \quad \text{for} \quad 0 < \theta <= 0.185, \text{and} \\ C_{\mathrm{surf}} &= 9\ 999\ 999 \quad \text{for} \quad \theta = 0. \end{aligned} \tag{16}$$

Clearly, generalization of this empirical model to other sites may require adjustment. In arid or sparsely vegetated environments where soil evaporation can be a significant component of the water balance, substitution of local empirical relationships may be necessary.

Final soil evaporation is a minimum of rates based on the Penman potential evaporation and soil exfiltration rates.

4.5. Capillary rise

Potential capillary rise is based upon the approach used by Eagleson (1978) such that

$$q_{\text{cap}} = K_{\text{sat}_{z_s}} \left[1 + \frac{1.5}{(1+3b)} \frac{\varphi_{\text{ae}}}{(z_s - \varphi_{\text{ae}})} \right]^{(2+3b)}, \tag{17}$$

where $K_{\text{sat}_{z_s}}$ is the hydraulic conductivity at the water table depth (z_s) [computed using Equation (8)]; b and φ_{ae} are pore size index and air entry pressure, respectively, and are set based on soil type.

Capillary rise is limited to filling unsaturated zone to field capacity. To correct for subdaily plant responses, one-half of the potential capillary rise, computed using Equation (17) is allocated to the unsaturated zone at the start of the day. The remaining potential is available later in the day to satisfy plant transpiration demands (see section 5.6.).

4.6. Snow accumulation and melt

Snow accumlation is based on incoming precipitation and is assumed to fall evenly over each climate zone. Modeling case studies using previous versions of RHESSys, however, have shown that in snow-dominated environments, the redistribution of snow by wind, can have a significant impact on hydrology (Hartman et al. 1999). In the current model, we do not account for this effect; however, an adaptation of a more sophisticated snow accumulation and melt approach will likely be included in future versions.

Snowmelt, q_{melt}, is computed using a quasi–energy budget approach that takes into account radiation (M_{rad}), a combination of melt due to sensible and latent heat flux (M_T), and advective (M_V) (from rain on snow) controls on snowmelt such that, at the daily time step

$$q_{\text{melt}} = M_{\text{rad}} + M_T + M_V. \tag{18}$$

Melt from temperature and advection occur only when the snowpack is ripe. Snowpack temperature is approximated using an air temperature accumulation of a snowpack energy deficit (SED):

$$\text{SED}_t = \max\left[\text{SED}_{(t-1)} + T_{\text{air}}, \text{SED}_{\text{max}}\right], \tag{19}$$

where $\text{SED}_{(t-1)}$ is the previous day's energy deficit, T_{air} is mean daily temperature, and SED_{max} is a maximum energy deficit that is set as a climate-region-specific input parameter. Melt due to radiation can occur as sublimation when the energy deficit SED is less than 0.

Radiation melt is computed as

$$M_{\text{rad}} = \frac{(K_{\text{direct}} + K_{\text{diffuse}} + L)}{\lambda_f \rho_{\text{water}}} \quad \text{for} \quad (\text{SED} >= 0),$$

$$M_{\text{rad}} = \frac{(K_{\text{direct}} + K_{\text{diffuse}} + L)}{(\lambda_f + \lambda_v)\rho_{\text{water}}} \quad \text{for} \quad (\text{SED} < 0), \tag{20}$$

where λ_v and λ_f are the latent heat of vaporization and and fusion, respectively; ρ_{water} is the density of water; K_{direct} and K_{diffuse} are direct and diffuse shortwave

radiation absorbed by the snowpack; and L is longwave radiation. Direct and diffuse shortwave radiation absorption by the snowpack is computed based on a Beer's law extinction model of available radiative fluxes ($K_{\text{direct}'}$ and $K_{\text{diffuse}'}$) and accounts for albedo-driven reflectance at the level of the snowpack. This approach is used to maintain consistency with radiation attenuation through vertical canopy layers as described in section 5.2. Thus,

$$K_{\text{direct}} = (1 - \alpha)K_{\text{direct}'}(1 - \exp^{-k_{\text{snow}}}). \tag{21}$$

The extinction coefficient k_{snow} is input as a climate-specific default. Setting k to an arbitrary large value will ensure that all nonreflected radiation will be absorbed by the snowpack. Snowpack reflectance or albedo α is estimated based upon a snowpack surface age following Laramie and Schaake (Laramie and Schaake 1972):

$$\begin{aligned} \alpha &= 0.85\left(0.82^{\text{Age}^{0.46}}\right) \quad \text{for} \quad (\text{SED} >= 0), \\ \alpha &= 0.85\left(0.94^{\text{Age}^{0.58}}\right) \quad \text{for} \quad (\text{SED} < 0), \end{aligned} \tag{22}$$

where "Age" is the number of days since last snowfall. A similar approach is used to account for diffuse radiation fluxes.

Longwave radiation into the snowpack is estimated from air temperature following Croley (Croley 1989):

$$\begin{aligned} L &= 41.868\left[\text{ess}_{\text{atm}}\sigma\,(T_{\text{air}} + 272)^4 - 663\right] \text{ for } (\text{SED} >= 0) \text{ and } (T_{\text{air}} >= 0), \\ L &= 41.868\left[(\text{ess}_{\text{atm}} - 1)\sigma\,(T_{\text{air}} + 272)^4 - 663\right] \text{ for } (\text{SED} < 0) \text{ and } (T_{\text{air}} < 0), \end{aligned} \tag{23}$$

where σ is the Stefan–Boltzmann constant. Atmospheric emissivity ess_{atm} is adjusted for overstory canopy (Dingman 1994) and cloud fraction (CF; Croley 1989):

$$\text{ess}_{\text{atm}} = (1 - F)\left[0.53 + 0.065\frac{{e_a}^{0.5}}{100}(1 + 4.0\text{CF}) + F\right], \tag{24}$$

where F is the fractional canopy cover over the snowpack and e_a is the atmospheric vapor pressure. If cloud fraction data are not available, the cloud fraction is assumed to be 1.0 for days with precipitation and 0.0 for dry days.

Melt due to latent and sensible heat flux is based on an empirical relationship with air temperature (Coughlan and Running 1997) that is adjusted for the effects of variation in wind speed due to the fractional forest cover F over a snowpack (Dunne and Leopold 1979)

$$M_T = \beta_{\text{MT}}T_{\text{air}}(1 - 0.8F), \tag{25}$$

where β_{MT} is an empirical temperature melt coefficient that is input as a climate-region-specific parameter.

Advection melt contributions due to warming by incoming precipitation are computed as

$$M_V = (\rho_{\text{water}}T_{\text{air}}\text{TFcp}_{\text{water}})/\lambda_f, \tag{26}$$

where TF is net throughfall entering the snowpack, and cp_{water} and ρ_{water} are the heat capacity and density of water, respectively.

4.7. Lateral redistribution

Soil moisture redistribution through saturated throughflow and associated runoff production can be modeled using either a quasi-spatially distributed model, TOPMODEL (Beven and Kirkby 1979) or via an explicit routing model, which is a modification of the Distributed Hydrology Soil Vegetation Model (DHSVM; Wigmosta et al. 1994).

TOPMODEL is applied at the hillslope level. DHSVM is applied at the basin level, since it can include some limited streamflow routing. Both approaches are executed at the end of the day, following vertical soil moisture updates.

4.7.1. TOPMODEL

TOPMODEL is a statistically based approach that redistributes saturation zone water based on an index of hydrologic similarity. As a statistically based approach, TOPMODEL represents a simplified approach that has been applied and tested in numerous catchments. TOPMODEL relationships are based on the assumption that saturated hydraulic conductivity varies exponentially with depth, that water table gradients can be approximated by local topographic slope, and that steady-state flux is achieved within the modeling time step. TOPMODEL distributes a mean soil moisture deficit, $\bar{s}$ based on a local wetness index w_i:

$$w_i = \ln \frac{\mathrm{ar} T_e}{T_o \tan\beta}, \tag{27}$$

where T_e and T_o are the mean and local hillslope saturated transmissivity, respectively, $\tan\beta$ is the local slope, and ar is the upslope contributing area.

Local saturation deficit s_i for each patch, is computed as

$$s_i = \bar{s} + m_s(\bar{w} - w_i), \tag{28}$$

where $\bar{w}$ is mean hillslope wetness index value, $\bar{s}$ is the mean hillslope saturation deficit, and m_s describes a decay rate of hydraulic conductivity with saturation deficit. Transmissivity TR is computed as

$$\mathrm{Tr} = \int_{-\infty}^{z_{\mathrm{sat}}} K_{\mathrm{sat}_0} \exp^{-\frac{s}{m_s}} dz, \tag{29}$$

where K_{sat_0} is saturated hydraulic conductivity at surface.

Alternatively, a constant or user-defined profile of hydraulic conductivity can replace the assumption of an exponential decay.

Saturation overland flow (return flow) is produced for patches if $(s_i < 0)$. Baseflow q_{base} for the hillslope is calculated as

$$q_{\mathrm{base}} = \exp^{(-\bar{w})} \exp^{(-\bar{s}')}, \tag{30}$$

where $\bar{s}'$ is the areally weighted mean of the saturation deficit of all hillslope patches adjusted to include a portion of the capillary fringe as follows:

$$-\bar{s}' = \sum_{i=1}^{n} \left[s_i - 0.5(\varphi_{\mathrm{ae}_i}) a_i / \mathrm{sum}_{i=1}^{n} a_i \phi_{0_a} \right], \tag{31}$$

where φ_{ae} is the air entry pressure, ϕ_0 is the porosity at the surface, s_i is the saturation deficit, and a_i is the area for patch i.

4.7.2. Explicit routing

Alternatively, the explicit routing model is based on the DHSVM (Wigmosta et al. 1994) routing approach that has been modified to account for nongrid-based patches and nonexponential transmissivity profiles. Similar to TOPMODEL, DHSVM assumes that hydraulic gradients follow surface topography. Flow topology is generated by a GIS-based preprocessing routine, CREATE-FLOWPATHS. Multiple flow directions, from any given patch, are permitted.

In the explicit routing approach, three distinct patch types are considered: streams, roads, and land surface. In the current implementation, stream patches include the riparian area adjacent to the stream. Thus vertical processes such as infiltration are modeled using the same algorithms applied for land surface patches. Lateral flow from the stream patch, however, is assumed be channelized. In the current implementation, all channelized flow is assumed to exit the basin in a single time step. Future implementation, however, will include an in-stream routing model between stream patches. Unique characteristics of lateral flow from road patches are discussed below.

Within the model time step, explicit routing is computed for a user-specified time step to achieve stability. This can be useful to maintain a Couret number less than 1 and reduce errors due to over/underestimation of downslope flood wave propagation. All vertical fluxes and storage adjustments including rainfall infiltration are done before the routing of lateral subsurface throughflow. If, however, hourly precipitation data are available, the vertical hydrologic flux portion of the model can be run at a corresponding hourly time step.

The DHVSM routing scheme assumes that saturated throughflow $q(t)_{a,b}$ from patch a to patch b can be estimated as

$$q(t)_{a,b} = \mathrm{Tr}(t)_{a,b} \tan\beta_{a,b} \omega_{a,b}, \tag{32}$$

where $\omega_{a,b}$ is the flow width between patches a and b, $\tan\beta$ is local slope, and Tr is transmissivity as defined in Equation (29).

For grids, flow widths are assumed to be 0.5 times the grid size for cardinal directions and 0.354 times the grid size for diagonal directions after Quinn et al. (Quinn et al. 1991). For irregular elements, flow widths are summed along the shared boundary between patches a and b.

Surface flow (i.e., saturation overland flow or Hortonian overland flow) produced is routed following the same patch topology used from routing saturated subsurface throughflow. All surface flow produced by a patch is assumed to exit from the patch within a single time step. If the receiving patch is not saturated, surface flow is allowed to infiltrate based on Equation (5) and is added to unsaturated soil moisture storage. Patch routing is sequenced to occur from the uppermost patches first.

Within the explicit routing model, patches that contain roads are treated as special cases.

4.7.3. Road patches

Roads have been shown to alter the routing of both overland and subsurface throughflow (Wemple et al. 1996; Luce and Cundy 1994). Road culverts produce channelized flow that in some cases can connect directly to the stream and effectively extend the stream drainage network. Flow in road culverts is produced from two sources: 1) runoff from the road surface and 2) interception of subsurface routing by the road cut bank. At present, patches can be parameterized using an areally weighted conductivity. If resolution is such that the road covers a significant portion of patch surface, then the infiltration capacity parameter assigned to that patch should reflect low infiltration capacities associated with roads.

The amount of saturated subsurface flow intercepted by the road is a function of the road cut depth and the current saturation deficit. If the road cut bank depth is less than depth to saturation, none of the saturated throughflow is intercepted by the road. If road cut depth is greater than depth to saturation, all subsurface throughflow produced *above* the road cut depth is captured by the road culvert.

Use of an alternative receiving patch allows flow intercepted by a road to be routed either to an adjacent patch or to a stream/storm network. The former represents the situation in which culverts serve to concentrate flow but allow this flow to be redistributed and reinfiltrated in down-slope patches. The latter models the case in which culverts form part of an extended drainage network. The location of patches to receive flow intercepted by culverts are specified as part of the routing topology in the CREATE-FLOWPATHS preprocessing routine prior to RHESSys execution. A new routing topology can be read in during execution, however, so that disturbances can be modeled.

4.7.4. Vertical and lateral redistribution of nitrate

In the current model, nitrate enters the soil from infiltrated rain or surface detention storage, using a mean concentration such that

$$\mathrm{soil}_{\mathrm{NO3}_t} = \mathrm{soil}_{\mathrm{NO3}_{t-1}} + \frac{q_i n\mathrm{fil}}{S_{\mathrm{det}} + P}\,\mathrm{surf}_{\mathrm{NO3}}, \tag{33}$$

where $\mathrm{soil}_{\mathrm{NO3}_{t-1}}$ and $\mathrm{soil}_{\mathrm{NO3}_t}$ are total soil nitrate at the previous and current time step, respectively; $q_i n\mathrm{fil}$ is infiltration; S_{det} is surface detention storage; P is precipitation; and $\mathrm{surf}_{\mathrm{NO3}}$ is the total mass of nitrate in surface detention storage and precipitation.

Vertical drainage of soluble nitrogen downward through the soil profile is not explicitly modeled in RHESSys. A simplified vertical redistribution is assumed based on a specified nitrate profile with depth. The current implementation assumes an exponential distribution such that

$$\mathrm{soil}_{\mathrm{NO3}} = \int_{z_0}^{z_{\mathrm{soil}}} \mathrm{NO3}_{\mathrm{surface}}\ \exp^{-\mathrm{N}_{\mathrm{decay}} z}, \tag{34}$$

soil_{NO3} is total mass of nitrate N in the soil profile, which is maintained as a state variable throughout the simulation. Here N_{decay} is a soil-specific parameter that defines the rate of decay of nitrate with depth and z_{soil} is soil depth. Equation (35) can be rearranged to determine N_{surface} and used to compute available nitrate N at any soil depth as

$$\text{soil}_{\text{NO3}_z} = \text{NO3}_{\text{surface}} \exp^{-N_{\text{decay}} z}. \tag{35}$$

Available nitrate N from Equation (35) is coupled with estimates of lateral saturated subsurface throughflow, Equation (32), to determine the total export of nitrate N from a given patch as

$$\text{NO3}_{\text{out}} = \int_{-\infty}^{z_{s z_{\text{soil}}}} \frac{q_z}{S_z} \text{soil}_{\text{NO3}_z} \text{NO3}_{\text{mobile}}, \tag{36}$$

where S_z is soil moisture (in meters of water) at depth z; z_s is saturation zone depth; q_z is net lateral transport of water from the patch at depth z; and $\text{NO3}_{\text{mobile}}$ is the portion of nitrate that is mobile (set as a soil-type parameter).

This approach to modeling nitrate export follows the flushing hypothesis. Use of an exponential profile distribution of nitrate, results in greater supplies of mobile N as saturation throughflow levels rise in the soil, and begin tapping more nutrient-rich near-surface soils. Field investigation of N-transport mechanisms (e.g., McDonnell 1990; Peters et al. 1995) suggests that this may be a reasonable assumption in areas, such as humid forests, where much of the infiltrating water rapidly moves through the unsaturated layer through preferential flowpaths, without significant matric contact. Further model development will investigate the marginal gains made by adopting a more rigorous vertical transport representation.

When using the TOPMODEL approach for soil moisture redistribution, the spatial variation in nitrate export is ignored. For model applications that focus on nutrient export in spatially heterogeneous terrain, the explicit routing option is therefore recommended. When TOPMODEL is used, a basin-scale-lumped approach is used to estimate mobile N transport. A mean hillslope soil nitrate storage is computed and used to determine a hillslope-scale nitrate export based on a mean basin saturation deficit following Equation (36) above. To account for losses due to lateral N export, all patches are assigned the updated mean basin soil nitrate value.

5. Canopy radiative and moisture fluxes

RHESSys models surface radiation and rainfall attenuation through a series of canopy layers.

In vegetated catchments, these layers correspond to overstory and understory vegetation. In urbanizing catchments, nonphotosynthesizing layers, such as buildings, can be represented to model the evaporation of intercepted water. For vegetated canopy, absorbed radiation also controls carbon/nitrogen cycling through photosynthesis and respiration. Carbon and nitrogen cycling are discussed in section 6.

Canopy layers are processed sequentially according to height. Radiation, wind, and rain or snow throughfall are attenuated as they are absorbed/intercepted by

each successive layer. Layers at equal height share the same environment. Canopy layers at the same height must have combined fractional coverage less than or equal to 1.

5.1. Leaf area and plant area index

Canopy layer leaf area index (LAI) reflects current leaf carbon storage cs.leaf, scaled by $\mathrm{LAI}_{\mathrm{sp}}$, specific leaf area index that varies with vegetation type.

Field evidence has shown that sunlit and shaded leaves respond differently in terms of photosynthetic efficiency, leaf nitrogen content, and specific leaf area (Thornton 1998). To account for this, we partition the canopy into sunlit and shaded components, following Chen et al. (Chen et al. 1999) such that

$$\begin{aligned} \mathrm{LAI}_{\mathrm{proj}_{\mathrm{sunlit}}} &= 2.0\,\cos(\Theta_{\mathrm{noon}})\left[1.0 - \exp^{-0.5(1-\mathrm{GF})\mathrm{LAI}_{\mathrm{proj}}/\cos(\Theta_{\mathrm{noon}})}\right], \\ \mathrm{LAI}_{\mathrm{proj}_{\mathrm{shade}}} &= \mathrm{LAI}_{\mathrm{proj}} - \mathrm{LAI}_{\mathrm{proj}_{\mathrm{sunlit}}}, \end{aligned} \tag{37}$$

where Θ_{noon} is the solar angle at noon and GF is the gap fraction. In addition to LAI, a total plant area index PAI is also required to account for the role played by stem wood in interception:

$$\mathrm{PAI} = \mathrm{LAI}_{\mathrm{proj}} + (\mathrm{cs.live.stem} + \mathrm{cs.dead.stem})\mathrm{swa}, \tag{38}$$

where cs.live.stem and cs.dead.stem are sapwood and heartwood stem carbon stores, respectively, and swa is a vegetation-specific parameter that defines stem wood equivalent area per unit of carbon. For grasses, PAI = LAI.

5.2. Radiation attenuation

Incoming direct and diffuse radiation at the top of the canopy is input directly or estimated as described in section 3.4. Canopy radiation attenuation and absorption by each canopy layer is modeled separately for diffuse, direct, and photosynthetically active radiation (PAR) radiative fluxes.

5.2.1. Direct radiation

Direct radiation interception is based on a modification of Beer's law with a correction for the effect of low sun angles in sparse canopies (Chen et al. 1997) such that

$$K_{\mathrm{direct}} = (1 - \alpha_{\mathrm{direct}})K_{\mathrm{direct}'}(1 - \exp^{-\mathrm{ext}_{\mathrm{coef}}}), \tag{39}$$

where α_{direct} is the vegetation-specific reflectance (albedo); K_{direct} is the absorbed direct radiation by the entire vegetation layer, including both leaves and stem wood; and $K_{\mathrm{direct}'}$ is the incoming direct radiation at the top of that canopy layer. The extinction coefficient $\mathrm{ext}_{\mathrm{coef}}$ is computed as

$$\mathrm{ext}_{\mathrm{coef}} = 1.1k\frac{(1 - \mathrm{GF})\mathrm{PAI}}{\cos(\Theta_{\mathrm{noon}})}, \tag{40}$$

where k is the vegetation-specific Beer's law extinction coefficient. For low values of the extinction coefficient a correction factor (Chen et al. 1997) is applied to

account for the effect of low sun angles in sparse canopies such that

$$K_{\text{direct}} = (1 - \alpha_{\text{direct}})K_{\text{direct}'}(1 - \text{corr}\ \exp^{-\text{ext}_{\text{coef}}}),$$
$$\text{corr} = (1 - \alpha_{\text{background}})\frac{(\Theta_{\text{noon}} - \frac{\Pi}{2})\ \sin(\Theta_{\text{noon}}) + \cos(\Theta_{\text{noon}})}{(\frac{\Pi}{2} - \Theta_{\text{noon}})[1 - \sin(\Theta_{\text{noon}})]}, \qquad (41)$$

where $\alpha_{\text{background}}$ is background (litter) reflectance and currently assumed to be equal to canopy reflectance.

5.2.2. Diffuse radiation

Total diffuse radiation absorption is computed based on the approach developed by Norman (1981) such that:

$$K_{\text{diffuse}} = (1 - \alpha_{\text{diffuse}})K_{\text{diffuse}'}\{1 - \exp^{-[(1-\text{GF})\text{PAI}]^{0.7}} + S_c\}, \qquad (42)$$

where α_{diffuse} is the vegetation-specific reflectance (albedo); GF is the gap fraction; K_{diffuse} is the direct radiation absorbed by the entire vegetation layer, including both leaves and stem wood; and $K_{\text{diffuse}'}$ is the incoming diffuse radiation at the top of that canopy layer. The scattering coefficient S_c is computed as

$$S_c = 0.07\frac{K_{\text{direct}'}}{K_{\text{diffuse}'}}[1.1 - 0.1(1 - \text{GF})\text{PAI}]\ \exp^{-\cos(\Theta_{\text{noon}})}. \qquad (43)$$

5.2.3. PAR radiation

Absorbed PAR ($\text{APAR}_{\text{direct}}$; $\text{APAR}_{\text{diffuse}}$) are calculated using Equations (41) and (42) above where reflectance coefficients, α and direct radiation extinction coefficients k are replaced by PAR-specific coefficients and LAI replaces PAI.

Radiation inputs per LAI, which are used to drive leaf conductance and photosynthesis submodels, are computed separately for sunlit ($\text{ppdf}_{\text{sunlit}}$) and shaded leaves ($\text{ppfd}_{\text{shade}}$).

5.3. Aerodynamic resistance

Aerodynamic resistance is computed separately for the top (overstory) canopy and understory layers following the model developed by Heddeland and Lettenmaier (Heddeland and Lettenmaier 1995). This model assumes a logarithmic wind speed decay profile to the top of the canopy and an exponential decay profile within the canopy. A patch-level stability correction is included based upon Oke (Oke 1987).

Overstory resistance ra_o is computed as

$$\text{ra}_o = \frac{\log\left[\frac{(z_{\text{sc}} - d_0)}{\text{zo}_0}\right]/0.41^2}{u^*}, \qquad (44)$$

where z_{sc} is the screen height; d_0 is the zero plane displacement of the overstory estimated as $0.7z_o$, where z_o is the overstory canopy height and zo_0 is the roughness length estimated as $0.1z_o$ and u^* is the friction velocity. To compute resistance of

understory layers, the wind speed profile must be estimated. Friction velocity is computed as

$$u_o = u^* \frac{\log\left(\frac{z_o - d_0}{\mathrm{zo}_0}\right)}{\log\left(\frac{z_s - d_0}{\mathrm{zo}_0}\right)}, \tag{45}$$

and then allowed to decay exponentially through canopy layers, until within $0.1\mathrm{zo}_0$, after which a logarithmic profile is assumed. Resulting estimates of understory resistance becomes

$$\mathrm{ra}_u = \mathrm{ra}_o + \log\frac{(z_s - d_0)}{\mathrm{zo}_0} z_o \exp^{-\mathrm{cn}} \frac{\left(\exp\left[-1(\mathrm{cn})\frac{(d_u + \mathrm{zo}_u)}{z_o}\right] - \exp\left[-1(\mathrm{cn})\frac{(d_0 + \mathrm{zo}_0)}{z_o}\right]\right)}{u^* 0.41^2 \mathrm{cn}(z_o - d_0)}$$
$$\text{for} \quad z_u > 0.1 z_o, \tag{46}$$

where cn is a vegetation-specific wind attenuation coefficient and d_u is the zero plane displacement of the understory. For understory layers less than $0.1z_o$, an additional term is added to Equation (46) so that

$$\mathrm{ra}_{u'} = \mathrm{ra}_u + \frac{\log\frac{(0.1 z_o)^2}{\mathrm{zo}_u}}{0.41^2 u^*}. \tag{47}$$

For additional understory layers, Equation (46) is repeated using successive values of canopy-layer heights for overstory and understory height (z_o and z_u) and wind speed, u^* following Equation (45).

5.4. Canopy conductance

Canopy conductance is computed separately for vascular and nonvascular layers. Vascular stratum conductance represents the inverse of additional resistance provided by stomatal control. Vascular stratum conductance is based upon the Jarvis multiplicative model of stratum conductance (Jarvis 1976) where maximum (plant specific) conductance is scaled by the environmental factors. To account for differences in radiative forcing, stomatal conductance is computed separately for sunlit ($\mathrm{gs}_{\mathrm{sunlit}}$) and shaded leaves ($\mathrm{gs}_{\mathrm{shade}}$):

$$\begin{aligned} \mathrm{gs}_{\mathrm{sunlit}} &= f(\mathrm{ppfd}_{\mathrm{sunlit}}) f(\mathrm{CO}_2) f(\mathrm{LWP}) f(\mathrm{vpd}) \mathrm{gs}_{\max}\left(\mathrm{LAI}_{\mathrm{proj}_{\mathrm{sunlit}}}\right), \\ \mathrm{gs}_{\mathrm{shade}} &= f(\mathrm{ppfd}_{\mathrm{shade}}) f(\mathrm{CO}_2) f(\mathrm{LWP}) f(\mathrm{vpd}) \mathrm{gs}_{\max}\left(\mathrm{LAI}_{\mathrm{proj}_{\mathrm{shade}}}\right), \end{aligned} \tag{48}$$

where $\mathrm{gs}_{\max}$ is the vegetation-type-specific maximum conductance. Functional relationships for environmental controls on stomatal conductance can be readily substituted in RHESSys. Current implementation of a 0–1 multipliers to reflect the influence of each environmental control—light [f(ppfd)], CO_2 [$f(CO_2)$], leaf water potential [f(LWP)], and vapor pressure deficit [f(vpd)]—are based on relationships developed by Running and Coughlan (Running and Coughlan 1988) for BIOME-BGC and are not shown here (with the exception of [f(LWP)]), which has been modified to reflect RHESSys approach to computing soil moisture conditions.

Leaf water potential is assumed to be a direct function of soil water tension Ψ, which is estimated based on soil moisture using either the Clapp and Hornberger

(Clapp and Hornberger 1978) approach where

$$\mathrm{LWP}_{\mathrm{predawn}} = \min\left[\mathrm{LWP}_{\mathrm{min.spring}}, -0.01\varphi_{\mathrm{ae}}(S^{-b})\right] \tag{49}$$

or the vanGenuchten and Nielsen (vanGenuchten and Nielsen 1984) approach where

$$\mathrm{LWP}_{\mathrm{predawn}} = \min\left[\mathrm{LWP}_{\mathrm{min.spring}}, -0.01\varphi_{\mathrm{ae}}\left(S^{\frac{1}{1-\frac{1}{b}}} - 1\right)^{\frac{1}{b}}\right]. \tag{50}$$

Air entry pressure φ_{ae} and pore size index b are parameters associated with a specific soil type. Here $\mathrm{LWP}_{\mathrm{min.spring}}$ is a vegetation-specific parameter, giving the leaf water potential when stomata are fully open. Here S is the rooting zone percent saturation. Leaf water potential control on stomatal conductance follows the approach used in BIOME-BGC.

Finally, the effect of CO_2 augmentation on stomatal conductance has not yet been implemented. Many field experiements have shown that increasing atmospheric CO_2 concentration may improve plant water use efficiency by reducing stomatal conductance (Medlyn et al. 2001). These relationships will be included in RHESSys in a subsequent version.

Nonvascular conductance

Nonvascular stratum conductance represents the inverse of additional resistance to surface vapor flux beyond aerodynamic conductance provided by a nonvascular layer. Note that this refers to nonvascular layers, such as mosses, rather than conductance from surface soil, which is discussed in section 4.4. The nonvascular conductance term is also used in the calculation of evaporation of intercepted water as discussed in section 5.6. below. Following Williams and Flanagan (1997) nonvascular conductance is based on an empirical linear relationship with water storage for boreal forest mosses:

$$\mathrm{gs}_{\mathrm{nonvas}} = \max(a_{g_{\mathrm{surf}}}\Theta_{I'} + b_{g_{\mathrm{surf}}}, 0.0). \tag{51}$$

Typical values for empirical parameters, $a_{g_{\mathrm{surf}}}$ and $b_{g_{\mathrm{surf}}}$, for mosses can be found in Williams and Flanagan (Williams and Flanagan 1997). Here $\Theta_{I'}$ is the relative interception storage by the layer, adjusted for potential evaporative losses during the day as follows:

$$\Theta_{I'} = \max\left[0, \frac{(2\Theta_I - 0.001)}{2\Theta_{I_{\max}}}\right], \tag{52}$$

where Θ_I is the current time step interception storage, and $\Theta_{I_{\max}}$ is a specific rain capacity scaled by PAI.

5.5. Interception

Canopy interception is a function of the water-holding capacity of the vegetation such that canopy interception CI is computed as

$$\mathrm{CI} = \max\{0.0, \min[(1 - \mathrm{GF})\mathrm{RT}, \mathrm{PAIcp}_{\mathrm{rain}} - \Theta_I]\}, \tag{53}$$

where Θ_I is the current time step interception storage; GF is the gap fraction; and cp_{rain} is the specific rain capacity (based on vegetation type). Here RT is rain throughfall from preceding canopy layers or incoming rainfall for the highest canopy layer. Snow interception is also computed using Equation (53) by substituting a specific snow interception capacity cp_{snow} and snow throughfall ST.

5.6. Evapotranspiration

Total evaporative fluxes from each canopy layer may include the evaporation of water intercepted by the canopy, sublimation of intercepted snow, and transpiration by vascular layers. Both evaporation and transpiration rates are computed using the standard Penman–Monteith equation (Monteith 1965).

For transpiration from sunlit and shaded portions of the canopy, canopy conductance gs is computed using Equation (48). For evaporation of surface water and nonvascular strata, such as mosses, $\text{gs}_{\text{nonvas}}$ is computed using Equation (51). Here R_{net} is net radiation computed as

$$R_{\text{net}} = K_{\text{direct}} + K_{\text{diffuse}} + L, \tag{54}$$

where K_{direct} andK_{diffuse} are computed for each layer using Equations (41) and (42), respectively; and L is the net longwave radiation. Note that transpiration for sunlit and shaded components of the canopy are computed separately, and R_{net} is adjusted to account for radiation intercepted by sunlit and shaded LAI.

Evapotranspiration rates are computed for rainy and dry periods of each day and the vapor pressure deficit is adjusted accordingly. Thus, if rainfall durations for each day are input into the model, total daily evaporation is computed as

$$\begin{aligned} E = \min\big[&\Theta_I, E_{\text{pot}}(\text{vpd} = 0; \text{gs} = \text{gs}_{\text{nonvas}})(D_{\text{rain}}) + \\ &E_{\text{pot}}(\text{vpd} = \overline{\text{vpd}}; \text{gs} = \text{gs}_{\text{nonvas}})(D_{\text{day}} - D_{\text{rain}})\big], \end{aligned} \tag{55}$$

where Θ_I is the current time step interception storage; D_{rain} is the daytime rain duration; D_{day} is the day length; and $\overline{\text{vpd}}$ is the daily average vapor pressure deficit.

Total transpiration Trp is computed as

$$\begin{aligned} \text{Trp} = {} & E_{\text{pot}}(\text{vpd} = 0; \text{gs} = \text{gs}_{\text{sunlit}}) + E_{\text{pot}}(\text{vpd} = 0, \text{gs} = \text{gs}_{\text{shade}}) \\ & \times (D_{\text{rain}}) + E_{\text{pot}}(\text{vpd} = \overline{\text{vpd}}; \text{gs} = \text{gs}_{\text{sunlit}}) \\ & + E_{\text{pot}}(\text{vpd} = \overline{\text{vpd}}; \text{gs} = \text{gs}_{\text{shade}})(D_{\text{day}} - D_{\text{rain}}). \end{aligned} \tag{56}$$

5.7. Litter interception and evaporation

Litter interception of net canopy rain throughfall RT is limited by a per-PAI maximum litter interception capacity ($\text{litter}_{\text{rain}_{\text{cap}}}$). The amount of interception per storm event can also be limited by a litter gap fraction GF in sparse canopies where litter does not cover the ground surface. Interception is computed as

$$\text{CI}_{\text{litter}} = \min\big\{\text{RT}(1.0 - \text{GF}), \big[\text{PAI}\big(\text{litter}_{\text{rain}_{\text{cap}}} - S_{\text{litter}}\big)\big]\big\}, \tag{57}$$

where S_{litter} is the current water content in litter.

In the current version, litter PAI is set to 1.0 if litter carbon storage is greater than 0 and 0 otherwise.

Evaporation from the litter is computed based on radiation available following attenuation through canopy layers. Evaporation is computed using the Penman approach, where gs is set to an arbitrarily large value (10 000) and ga is based on a reduction of wind speed through the canopy to the litter layer as discussed in section 5.3.

Note that in cases where detention storage capacity is greater than 0, water in excess of litter interception capacity may be collected at the surface and evaporated.

6. Carbon and nitrogen cycling

The main structure of carbon cycling in RHESSys is based on BIOME-BGC (Thornton 1998) although many of the specific algorithms have been extended and/or modified.

Carbon and nitrogen cycling associated with live vegetation (e.g., photosynthesis, respiration) is included in canopy strata object routines. Carbon and nitrogen cycling associated with litter and soil layers (e.g., decomposition) occurs within patch objects. Thus, all vegetation strata associated with a particular patch contribute and extract material (carbon, water, and nitrogen) to and from the same well-mixed soil and litter pools.

RHESSys carbon and nitrogen stores are partitioned into leaves, roots, stems, and coarse roots. Stem and coarse-root stores also include both live and dead wood components to account for differences in respiration and C:N ratios. For grasses, stores are restricted to leaves and fine roots and include an additional store used to account for dead biomass that remains standing. Vegetation nitrogen stores follow carbon stores based on stoichiometric relationships discussed in more detail below.

6.1. Vegetation: Carbon cycling

6.1.1. Photosynthesis

Carbon enters the system through photosynthesis. The Farquhar model (Farquhar and vonCaemmerer 1982) calculates photosynthesis based on limitations due to enzymes (i.e., nitrogen), electron transport (i.e., light), and stomatal conductance (i.e., light and water) such that the net assimilation rate per unit LAI, A is

$$A = f(\mathrm{lnc}, \mathrm{irad}, \mathrm{gs}, p_a, \mathrm{CO_2}, T_{\mathrm{day}}), \tag{58}$$

where gs is the stomatal conductance, p_{a} is the atmospheric pressure, $\mathrm{CO_2}$ is the atmospheric carbon dioxide concentration, T_{day} is the daytime average air temperature, and lnc is leaf nitrogen concentration computed. Here irad is the net incoming radiation per unit LAI, which is computed as

$$\mathrm{irad} = (\mathrm{APAR}_{\mathrm{direct}} + \mathrm{APAR}_{\mathrm{diffuse}})/\mathrm{LAI}_{\mathrm{proj}}/\mathrm{time\ step}, \tag{59}$$

Note that the Farquhar model computes an assimilation rate per unit LAI. For the daily time step, to determine total daily canopy photosynthesis, g_{psn}, the mean

absorbed PAR, mean stomatal conductance, and daytime temperature are used to compute a mean assimilation rate that is then scaled by day length and LAI to yield total gross daily canopy photosynthesis. To account for nonlinearities in the responses of sunlit and shaded leaves, assimilation rates are computed separately so that total gross daily canopy photosynthesis, g_{psn}, for the strata becomes

$$g_{\text{psn}} = (A_{\text{sunlit}}\text{LAI}_{\text{sunlit}} + A_{\text{shaded}}\text{LAI}_{\text{shaded}})\text{dayl}. \quad (60)$$

Sunlit and shaded proportion of LAI are computed using (37). A summary of the specific equations used in the Farquhar model can be found in Waring and Running (Waring and Running 1998).

Finally, the Farquhar model takes into account the control exerted by the leaf nitrogen content. Photosynthesis is also constrained by the amount of nitrogen in the soil that is available for uptake by the plant. As computed, g_{psn} is a potential photosynthesis subject to the availability of nitrogen. The amount of nitrogen required, however, depends upon the allocation strategy used by the plant since different plant components (i.e., leaves versus stems) have different C:N ratios. The allocation strategy is discussed in section 6.1.4. below. Total nitrogen required from the soil, potential.plant.N.uptake, is determined based on g_{psn} and the allocation strategy. If sufficient mineralized nitrogen is available, g_{psn} is used for plant allocation. If, however, nitrogen is limiting, g_{psn} is reduced until the nitrogen requirements can be met. Section 6.3.1. discusses how soil nitrogen availability is determined.

6.1.2. Respiration

As in BIOME-BGC total maintenance respiration total_{mr} integrates respiration for each live carbon store including leaves, roots, and stems. Respiration for each component is computed as a function of nitrogen concentration and the current air temperature using the model developed by Ryan (Ryan 1991).

Growth respiration is also computed and subtracted from the carbon allocated to each vegetation component. Growth respiration is computed as a fixed percentage gr_{perc} of new carbon allocation, where gr_{perc} is a strata-specific (i.e., vegetation type) parameter. Ryan (Ryan 1991) suggests a growth respiration rate gr_{perc} of 25% for trees.

6.1.3. Phenology

In RHESSys, as in BIOME-BGC, net photosynthesis can be allocated on a daily or annual basis. Each day, net_{psn} is partitioned to the various tissues (leaves, roots, and stems). Partitioning between these various tissues is discussed below. The vegetation-type parameter alloc.prop.day.growth sets the percentage of newly assimilated carbon, which is expressed on a daily basis. The remaining carbon is stored and expressed during an annual leaf-out period. For deciduous trees and grasses, alloc.prop.day.growth must be substantially less than 1 to ensure enough stored carbon for spring leaf out. The timing and length of the annual leaf out period is also set in the vegetation-type parameter file, using parameters day.leaf.on

and ndays.expand, respectively. Note that although this period is referred to as leaf out, it also controls the assimilate allocated annually to roots. Carbon stored for annual allocation from the previous year is expressed during the leaf-out period. For each day during the leaf-out period, stored carbon is transferred to leaf and fine root pools such that amounts transferred to each component decreases linearly over each day of the leaf-out period.

In addition to annual leaf-out periods, leaf and fine root turnover periods are defined, again using a fixed timing set by stratum-specific parameters (day.leaf.off and ndays.litfal). The amount of leaf and fine root carbon transferred to the litter pool during this period is a fixed percentage (leaf.turnover and froot.turnover, respectively) of current leaf and fine root carbon pools. Parameters are set in a stratum parameter file. For deciduous trees, however, the entire leaf carbon pool is transferred to the litter pool. For grasses, the leaf carbon pool is first transferred to a standing dead leaf carbon pool, which acts as an intermediate store. Transfer from standing dead leaf carbon to the litter pool occurs at the rate defined by $\text{deadleaf}_{\text{turnover}}$ (percentage of dead leaf turnover per year). For all vegetation types, the amounts of leaf and fine root turnover during the fall turnover period follows a linearly decreasing daily transfer schedule similar to that used for leaf out during the spring.

Future versions of RHESSys will incorporate a variable phenology model (i.e., White et al. 1997) to account for environmental (i.e., temperature, radiation, etc.) controls on the timing of spring leaf out and fall leaf drop. This will also allow the model to account for plant responses to environmental stress through increases in leaf fall.

Different vegetation types show different sensitivities to daily versus annual allocation and the timing of phenology. Conifers, because they lose only a portion of their leaves, are less sensitive. For deciduous trees and grasses, some portion of photosynthesis must be reserved for annual allocation (i.e., alloc.prop.day.growth must be less than 1) to restart photosynthesis during the spring and these vegetation types are typically more sensitive to phenology timing.

For trees, the sapwood components of stem and coarse root pools must also be transferred to heartwood stem and coarse root pools. The rate of sapwood to heartwood turnover is also based on a fixed percentage ($\text{livewood}_{\text{turnover}}$) of the associated sapwood pools. Loss of carbon from heartwood pools can only occur due to whole tree mortality (discussed below).

6.1.4. Allocation

New net photosynthesis must be partitioned between roots, stems, and leaves or in the case of grasses, between roots and leaves. BIOME-BGC (Thornton 1998) maintains a fixed partitioning strategy such that the ratio of carbon allocated to each store is constant and set by species-specific parameters.

In RHESSys, a variable partitioning strategy based on Landsberg and Waring (Landsberg and Waring 1997) has been included to reflect the impact of soil moisture and nutrient stress on plant leaf to root allocation ratios. The fraction of the new assimilate that is allocated to roots depends on the ratio of actual to potential photosynthesis such that more carbon is allocated to roots when water or

nutrient limitations reduce actual photosynthesis. The fraction allocated to roots f_{root}, is computed as

$$f_{root} = 0.8/\left\{1 + 2.5\left[(psn_{pot}/psn_{actual})\right]\right\}, \quad (61)$$

where psn_{pot} and psn_{actual} are computed using Equation (58) such that for psn_{pot}, stomatal conductance and leaf nitrogen concentration values are set to the maximum given by species-specific parameters. For psn_{actual}, actual stomatal conductance [see Equation (48)] and the actual lnc are used.

Once the fraction allocated to roots has been determined, the remaining assimilate is allocated to leaves and, in the case of trees, stem wood based on a fixed ratio ($alloc_{stemc.leafc}$). For trees, carbon allocated to stem wood is further partitioned into coarse-root and stem components and further into live and dead wood components based on fixed ratios ($alloc_{crootc.stemc}$ and $alloc_{livewood.woodc}$, respectively).

Finally once fractions to be allocated to each plant component have been determined, the total amount of carbon allocated to leaves is then given as

$$c_{pool}.to.leaf_c = nlc(plant.c_{alloc})f_{leaf} \quad (62)$$

and

$$c_{pool}.to.leaf_c.store = (1.0 - nlc)(plant.c_{alloc})f_{leaf}, \quad (63)$$

where $plant.c_{alloc}$ is the total carbon available for allocation, nlc is the percentage to be allocated daily, $c_{pool}.to.leaf_c$ is carbon allocated to leaves on that day, and $c_{pool}.to.leaf_{cstore}$ is additional carbon to be allocated to leaves during the next leaf-out period.

Allocations to fine and coarse roots and stems follow a similar approach.

6.1.5. Alternative allocation strategy

Finally, there is considerable uncertainty in current models of plant carbon allocation strategies. To explore the implications of uncertainty, we have included an alternative approach to carbon allocation, which can be substituted by the user. Dickenson et al. (Dickenson et al. 1998) developed an allocation approach that reflects changes in allocation strategy in response to changing average canopy light levels as vegetation develops. This approach computes the fraction of assimilate allocated to leaves as follows:

$$f_{leaf} = \exp^{(-2.5LAI)}. \quad (64)$$

For trees, partitioning between roots and wood (coarse root and stem) is calculated such that the ratio of root to wood carbon (C_{root}/C_{wood}) approaches a constant:

$$f_{root} = 1/\beta \exp^{(-r_w \beta C_{root}/C_{wood})}, \quad (65)$$

where r_w and β are species-specific empirical constants.

Once these initial allocation fractions are computed, the impact of soil nitrogen limitations and finally allocation amounts are computed using the same approach described above.

6.1.6. Mortality

An annual plant mortality rate as a fixed percentage of current biomass is set in the stratum parameter file (mortality). Total carbon and nitrogen to be lost due to plant mortality is set each year. The same percentage is taken from each of the available tissue stores (i.e., leaves, roots, stem). Carbon that is lost from leaves and fine roots is transferred to the litter pool. Coarse stem and root material is transferred to a coarse wood debris pool that decays at a species-specific fragmentation rate before it is transferred to litter carbon and nitrogen pools. Fragmentation does not alter wood C:N ratios.

Material transfers due to mortality occur on a daily basis such that the annual plant mortality rate is maintained. The annual rate is reset each year (at the start of leaf out) to respond to changes in available stores. Future versions of RHESSys may incorporate a variable mortality rate as a function of environmental stressors that increase susceptibility to disease, blow down, etc. In the current version, episodic changes in vegetation such as forest harvesting or fire can be implemented through a dynamic redefinition of the stratum-level carbon- and nitrogen-state variables. An independent disturbance model can be used to determine size and frequency of these events.

6.2. Vegetation: Nitrogen cycling

In general, the cycling of nitrogen within the vegetation is tied stoichiometrically to that of carbon. In RHESSys, the C:N ratios of the various plant biomass components are fixed based on species-specific input parameters. A number of studies have shown that plants may vary biomass C:N ratios, particularly of leaves, in response to environmental stress (Aber and Melillo 1991). Thornton (Thornton 1998), on the other hand, summarizes studies that suggest that plants respond to nitrogen limitations through variations in total leaf area and leaf area per unit of nitrogen. At present, we follow the BIOME-BGC approach and hold leaf and other C:N ratios constant. Within the simulation, however, carbon and nitrogen stores and fluxes are maintained separately to facilitate future implementation of algorithms to account for differences in C:N ratios in response to stress.

One exception to the above implementation occurs during leaf fall. Retranslocation of leaf nitrogen as leaves fall results in increased C:N ratios in litter fall and excess nitrogen stored within the plant. This retranslocated stored nitrogen is then available for plant use during subsequent growth (i.e., in addition to nitrogen available through uptake from the soil). Separate parameters are therefore required to set leaf litter and leaf C:N ratios.

6.3. Soil

6.3.1. Decomposition

Daily soil and litter decomposition models are based on an approach developed by Thornton (Thornton 1998) for use in BIOME-BGC, which is similar to the approach used by CENTURY (Parton et al. 1996). Decomposition is based on a set of litter and soil pools, each of which includes both organic material and microbial biomass. Each pool is associated with a specific C:N ratio and a

potential decay rate. This decay rate includes both carbon lost due to microbial respiration and carbon transferred to the next soil/litter pool. Respiration is computed as a percentage of decomposition rates and are specific to each soil/litter pool (based on Thornton 1998).

The potential decay rate associated with each soil or litter pool may be reduced as a function of soil moisture, temperature, and nitrogen limitations. Scalar multipliers for temperature and moisture effects (w_{scalar} and t_{scalar}, respectively) are computed as follows:

$$t_{\text{scalar}} = \exp^{308.56\left[\frac{1}{71.02}-\frac{1}{(T_{\text{soil}}+273.15-227.13)}\right]} \quad \text{for} \quad T_{\text{soil}} > -10,$$
$$t_{\text{scalar}} = 0.0 \quad \text{for} \quad T_{\text{soil}} \leq -10. \tag{66}$$

The equation used for soil moisture effects differs from that used in BIOME-BGC in order to account for the reduction of decomposition rates in saturated soils. While Thornton's (Thornton 1998) approach assumed a well-drained soil environment, RHESSys adjusts decomposition rates following the modifier used by Parton et al. (Parton et al. 1996) to model soil moisture controls on nitrification:

$$w_{\text{scalar}} = \frac{(\theta - b)^{d\left[\frac{(b-a)}{(a-c)}\right]}}{(a-b)} \frac{(\theta - c)^{d}}{(a-c)}, \tag{67}$$

where a, b, c, d are soil parameters and θ is soil moisture.

Availability of mineralized nitrogen may also impact decay rates. Once the potential decomposition rates have been adjusted for each soil and litter pool, total immobilization and mineralization fluxes (i.e., from all pools) are computed based on relative C:N ratios associated with soil/litter pool transfers. If net immobilization flux (i.e., total immobilization − mineralization) is greater than currently available mineralized nitrogen store, immobilizing decomposition fluxes are proportionally reduced. Note that potential competition with plant nitrogen uptake must also be taken into account here. Thus, in the case of nitrogen limitation, plant uptake and immobilizing decomposition rates are reduced proportionally such that

$$\text{sum.N.demand} = \text{potential.plant.N.uptake} + \text{potential.soilN.immobilized},$$
$$\text{actual.plant.N.uptake} = \frac{\text{potential.plant.N.uptake}}{\text{sum.N.demand}}(\text{soil.N.avail}),$$
$$\text{actual.soilN.immobilized} = \frac{\text{potential.soilN.immobilized}}{\text{sum.N.demand}}(\text{soil.N.avail}). \tag{68}$$

Note that soil.N.avail includes both mineralized N from soil decomposition and any additional soil.NH_4 or soil.NO_3 from fertilization, nitrogen deposition, or N fixation.

6.3.2. Nitrification

Mineralized nitrogen soil.sminn that is made available through organic matter decomposition is assumed to be ammonia, soil.NH_4. Nitrification may transform soil.NH_4 into soil.NO_3. Potential nitrification rates are based on the approach developed and tested by Parton et al. (Parton et al. 1996) as part of the

$\text{CENTURY}_{\text{NGAS}}$ model. The nitrification rate N_{nitrif}, is a function of soil moisture (f_{H_2O}), carbon substrate availability (soil.sminn), soil temperature (f_T), and available soil.NH_4 such that

$$N_{\text{nitrif}} = f_{H_2O} f_T f_{NH_4} \text{soil.sminn}, \tag{69}$$

where f_{H_2O} is computed following the same approached used to calculate w_{scalar} in Equation (67) and temperature control f_T is computed as

$$f_T = 0.06 + 0.13 \exp^{0.07 T_{\text{soil}}}, \tag{70}$$

where T_{soil} is the soil temperature.

Concentration of ammonium controls the rate of nitrification such that

$$f_{NH_4} = 1.0 - \exp^{[-0.0105(NH_{4\text{conc}})]}, \tag{71}$$

where $NH_{4\text{conc}}$ is soil ammonium concentration in the organic soil layer.

Only mineralized soil nitrogen (i.e., from the decomposition of soil organic material; soil.sminn or fertilizer) is used for nitrification. This ensures the availability of soil carbon for the microbial nitrification processes (Gold et al. 2001).

6.3.3. Denitrification

Nitrate can be lost from the soil through flushing and/or denitrification. Flushing of nitrate through lateral subsurface throughflow is discussed in section 4.7.4. Denitrification is also modeled using the approach used in the $\text{CENTURY}_{\text{NGAS}}$ model (Parton et al. 1996). Denitrification N_{denitrif} is a function of a maximum denitrification rate (R_{NO_3}) based on available soil nitrate. This maximum rate is then modified by soil moisture and soil respiration such that

$$N_{\text{denitrif}} = f_{H_2O} f_{\text{hr}_{CO_2}} R_{NO_3}. \tag{72}$$

Maximum denitrification R_{NO_3} is computed as

$$R_{NO_3} = 0.0011 + \frac{\arctan[\Pi 0.002 \frac{(NO_3.\text{soil})}{N_{\text{soil}} + C_{\text{soil}}} - 180]}{\Pi}, \tag{73}$$

where (NO_3.soil) is available nitrate in the soil and N_{soil} and C_{soil} are soil nitrogen and carbon masses, respectively.

Soil moisture limitation f_{H_2O} is computed as

$$f_{H_2O} = \frac{a}{b^{\frac{c}{d\theta}}}, \tag{74}$$

where *a, b, c, d* are set as a function of soil texture as described in Parton et al. (Parton et al. 1996).

The soil (heterotrophic) respiration rate (hr_{CO_2}) is used as an index of carbon availability, which has been shown to limit microbial denitrification:

$$f_{\text{hr}_{CO_2}} = \frac{0.0024}{1 + \frac{200}{\exp^{0.35 \text{hr}_{CO_2}}}} - 0.0001, \tag{75}$$

where hr is total soil respiration rate, which is calculated as discussed in section 6.3.1.

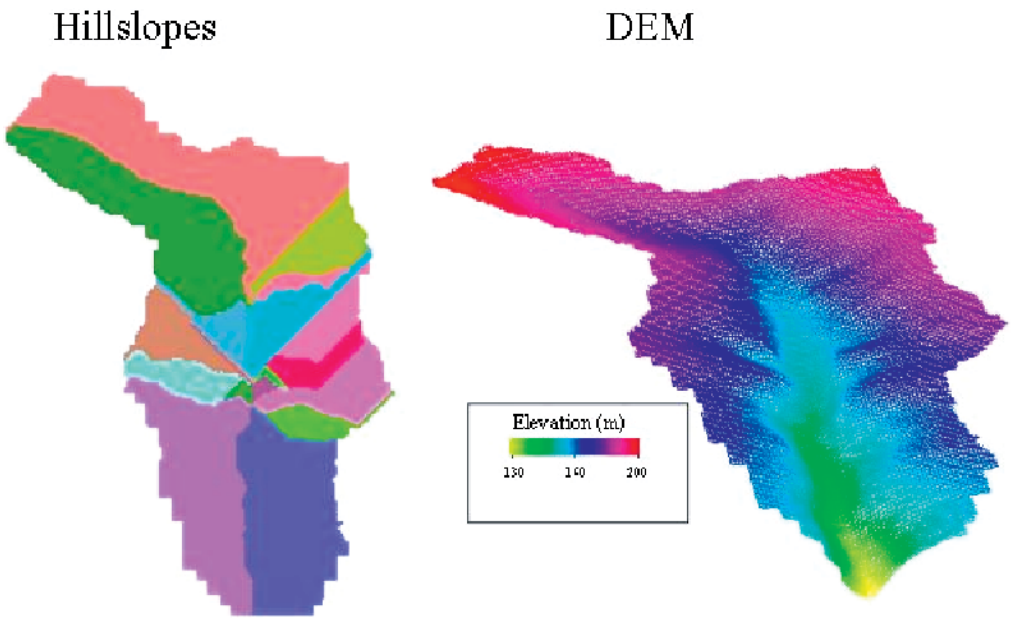

Figure 2. Hillslope delineation and 30-m DEM for Pond Branch.

7. Application: Hydrologic controls on N cycling for a small forested catchment

Specific applications of RHESSys highlight different components of model structure and function. Hydrologic applications of this model focus on predictions of streamflow and spatial patterns of soil moisture under a variety of land-cover and climate forcing conditions. Biogeochemical applications have used the model to examine the mechanisms that control the cycling and transport of both carbon and nitrogen within a watershed. As an example, a brief overview of a current RHESSys application is presented here. Additional detail on this study can be found in Band et al. (Band et al. 2001).

Pond Branch is a 34-ha catchment used as the control forested catchment as part of the Baltimore Long-Term Ecological Research program. As part of this project, continuous streamflow and weekly stream chemistry have been monitored since fall 1998. Watershed topography is characterized by a gently sloping upland area with steep side slopes draining to a broad riparian area. Upland soils are silt loam soil with underlying deep saprolite. Side slopes contain very shallow soils, while the bottomland is characterized by a substantial organic soil layer. Vegetation is dominated by a mature oak–hickory forest.

Because this is a relatively small watershed, patches were based on 5-m pixels. Hillslope delineation is shown in Figure 2. Soil parameters appropriate for sandy loam and vegetation parameters for an oak–hickory forest were used. When RHESSys is run in dynamic mode (i.e., soil and vegetation are not prescribed but are computed by the model), the model must be run for a period of spinup to generate carbon and nitrogen pools. In this case, the model was spun up for 200

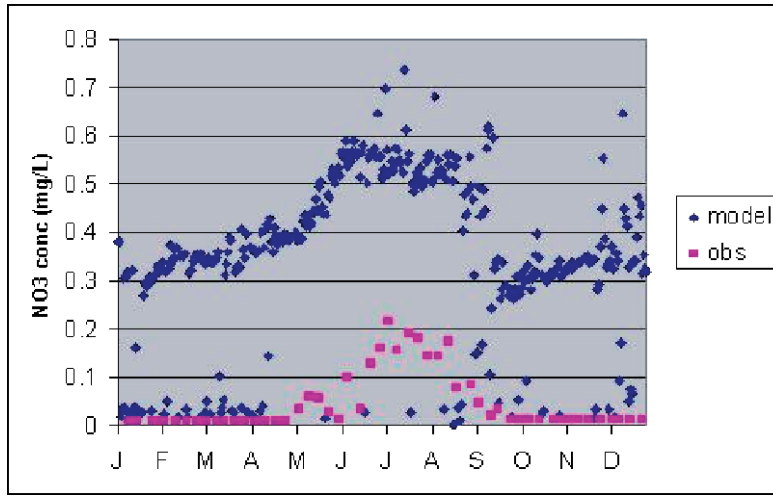

Figure 3. RHESSys and measured stream nitrate concentrations (mgN L^{-1}) for Pond Branch during Jan 1999–Dec 2000.

years, at which point both canopy cover and soil carbon pools had stabilized (i.e., reached equilibrium values). Once stable carbon and nitrogen pools were achieved, United States Geological Survey (USGS) stream gauge records were used to calibrate the model by varying $K\text{sat}_0$, hydraulic conductivity at the surface and m, the decay of hydraulic conductivity with depth. Calibration used a Monte Carlo–

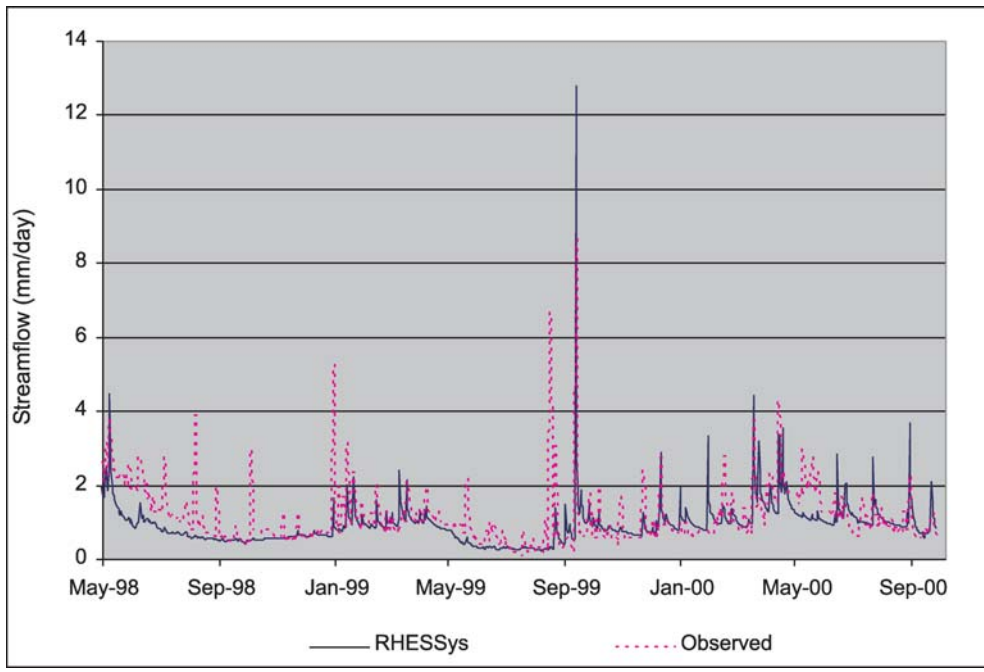

Figure 4. RHESSys and measured streamflow (normalized by drainage area) for Pond Branch.

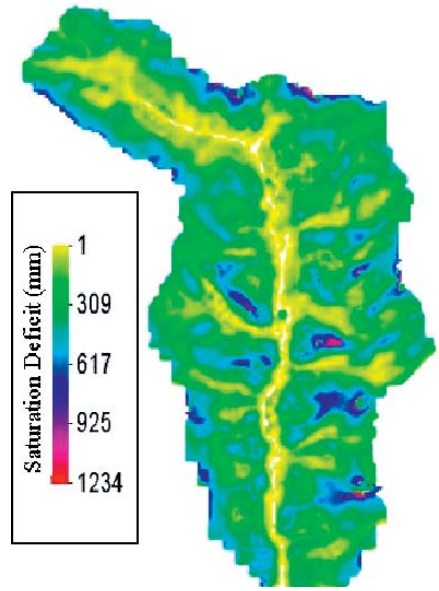

Figure 5. RHESSys saturation deficit (mm of water) for Pond Branch in Aug 2000.

based approach to run the model over a range of values for m and K. The set of values producing the optimal correspondence between observed and modeled streamflow as measured by the highest Nash–Sutcliffe efficiency (Nash and Sutcliffe 1970) were selected for future runs.

Correspondence between modeled and observed streamflow as well as modeled and observed stream nitrate concentration illustrate both the strengths and weakness of RHESSys application in this particular watershed (see Figures 3 and 4). As discussed in an earlier paper (Band et al. 2001), RHESSys tends to overpredict nitrate concentration in this watershed, although it captures the temporal pattern of nitrate export. RHESSys does not model in-stream processes, thus overprediction of the nitrate export may suggest that in this watershed in-stream losses are significant. Field data collected as part of this project support this conclusion. One of the surprising patterns in both field and modeled nitrate export is the increase in N concentration during the summer when biologic activity and hence biologic uptake of nitrogen is typically high. RHESSys output was used to help explain this pattern. Examining spatial outputs show that this increase in nitrification occurs primarily in the riparian region as it dries out during the summer period. The location of these processes within the riparian zones, which maintain connectivity to the stream throughout the summer, is important. Examining RHESSys spatial patterns of soil moisture illustrates temporal and spatial variation in surface saturated areas in which riparian zone processes occur (Figure 5). Modeled spatial patterns of soil moisture suggest that in addition to the classically defined riparian zone, topographic hollows, which drain into the riparian area, are also areas of significant saturation during parts of the year. These spatial patterns suggest that these topographic hollows may play a role similar to the riparian area in terms of both overall control on hydrology and nitrogen cycling, at least during the wetter periods. These results further suggest areas where additional

field study may be needed to collect data in these areas, which potentially act as controls on water quality and quantity in this watershed.

Acknowledgments. The Baltimore Ecosystem Study project is supported by the NSF Grant GRS 0095796 to L. Band and C. Tague, and National Science Foundation Long-Term Ecological Research program Grant DEB 9714835. We thank the USDA Forest Service Northeastern Research Station and BES for site management. In addition we thank the University of Maryland, Baltimore County, for their contribution of office and laboratory space at the Research Technology Center. We also thank the Baltimore Department of Parks and Recreation and Department of Public Works, the Baltimore County Department of Parks, and the Maryland Department of Natural Resources for their support.

APPENDIX: RHESSys Variables

This appendix lists the current atmospheric variables that are used internally in the RHESSys model.

A1. Environmental time series inputs.

Variable	Description
Rain	Precipitation (rain + snow), required
T_{min}	Minimum daily temperature, required
T_{max}	Maximum daily temperature, required
T_{day}	Mean daytime temperature
$T_{night_{max}}$	Night time temperature at sundown
T_{soil}	Soil temperature
dayl	Day length
daytimerainduration	Duration of rainfall
LAIscalar	Zone and seasonal scaling of LAI
L	Incoming longwave radiation
K_{direct}	Incoming direct shortwave radiation
$K_{diffuse}$	Incoming diffuse shortwave radiation
$PAR_{diffuse}$	Incoming direct PAR radiation
PAR_{direct}	Incoming diffuse PAR radiation
rel$H$	Relative humidity
vpd	Vapor pressure deficit
u*	Wind speed
$ndep_{NO_3}$	Nitrate deposition
$ndep_{NH_4}$	Ammonium deposition

A2. The RHESSys variable list.

Variable	Description	Units
a	Empirical soil parameter	DIM
A	Net assimilation rate	μmol m^2 s^{-1}
α	Snowpack albedo	0–1
α_{direct}	Vegetation reflectance (direct radiation)	0–1
$\alpha_{background}$	Background (litter) reflectance	0–1
$\alpha_{diffuse}$	Vegetation reflectance (diffuse radiation)	0–1

A2. (*Continued*)

Variable	Description	Units
A_{sunlit}	Sunlit assimilation rate	μmol m^2 s^{-1}
A_{shaded}	Shaded assimilation rate	μmol m^2 s^{-1}
$a_{g_{surf}}$	Empirical moss parameter	DIM
a_i	Area for patch	m^2
Age	Age of snowpack surface	Days
$alloc_{crootc.stemc}$	Ratio of carbon allocated to coarse root and stem	Ratio
$alloc_{livewood.woodc}$	Ratio of carbon allocated to live and dead wood	Ratio
$APAR_{direct}$	Absorbed photosynthetically active direct radiation	μmol m^2 day^{-1}
$APAR_{diffuse}$	Absorbed photosynthetically active diffuse radiation	μmol m^2 day^{-1}
ar	Upslope contributing area	m^2
b	Pore size index	DIM
b	Empirical soil parameter	DIM
β_{MT}	Empirical temperature melt coefficient	DIM
β	Species specific empirical constant	DIM
c	Pore disconnectedness index	DIM
c	Empirical soil parameter	DIM
C_{soil}	Soil carbon mass	kgC m^{-2}
$c_{pool.to.leaf_c}$	Total amount of carbon allocated to leaves	kg m^2 day^{-1}
$c_{pool.to.leaf_{c_{store}}}$	Carbon to be allocated to leaves during the next leaf out period	kg m^2
C_{surf}	Surface conductance for soil	m day^{-1}
CF	Cloud fraction	%
CI	Canopy interception	m
CI_{litter}	Litter interception	m
cn	Vegetation specific wind attenuation coefficient	0 − 1
CO_2	Atmospheric carbon dioxide concentration	ppm
cp_{rain}	Specific rain interception capacity	m
cp_{snow}	Specific snow interception capacity	m
cp_{water}	Heat capacity of water	kJ kg K^{-1}
cs.dead.stem	Heartwood stem carbon store	kg m^2
cs.live.stem	Sapwood stem carbon store	kg m^2
d	Empirical soil parameter	DIM
d_0	Zero plane displacement	m
D_{day}	Day length	s
D_{rain}	Daytime rain duration	s
d_u	Understory zero plane displacement	m
dayl	Daylength	s
$daytime_{rain_{duration}}$	Duration of rainfall	s
det$S$	Surface detention storage	m
E	Total daily evaporation	m day^{-1}
E	Evaporation	m day^{-1}
e_a	Atmospheric vapor pressure	Pa
ess_{atm}	Atmospheric emissivity	Pa
ET_{sat}	Evapotranspiration from the saturated zone	m day^{-1}
ET_{unsat}	Evapotranspiration from the unsaturated zone	m day^{-1}
ext_{coef}	Canopy radiation extinction coefficient	0 − 1
F	Fractional canopy cover over the snowpack	%
f_{leaf}	Fraction of assimilate allocated to leaves	%
f_{root}	Fraction of assimilate allocated to roots	%
g_{psn}	Gross daily canopy photosynthesis	kgC m^2 day^{-1}
GF	Gap fraction	0 − 1
gr_{perc}	Percentage of NPP to growth respiration	%
gs	Canopy conductance	m s^{-1}

A2. (*Continued*)

Variable	Description	Units
gs_{max}	Vegetation type specific maximum conductance	m s^{-1}
gs_{nonvas}	Nonvascular conductance	m s^{-1}
gs_{sunlit}	Sunlit stomatal conductance	m s^{-1}
gs_{shade}	Shaded stomatal conductance	m s^{-1}
hr_{CO_2}	Soil (heterotrophic) respiration rate	kgC m^2 day^{-1}
I	Rainfall intensity	m day^{-1}
irad	Net incoming radiation	μmol m^2 s^{-1}
k	Vegetation-specific Beer's law extinction coefficient	0 − 1
$K_{diffuse}$	Absorbed diffuse shortwave radiation	kJ m^2 day^{-1}
$K_{diffuse'}$	Incoming diffuse shortwave radiation	kJ m^2 day^{-1}
K_{direct}	Absorbed direct shortwave radiation	kJ m^2 day^{-1}
$K_{direct'}$	Incoming direct shortwave radiation	kJ m^2 day^{-1}
K_{sat_0}	Saturated hydraulic conductivity at the surface	m day^{-1}
K_{sat_s}	Saturated hydraulic conductivity	m day^{-1}
K_{snow}	Snowpack radiation extinction coeff	0 − 1
K_{unsat}	Vertical unsaturated hydraulic conductivity	m day^{-1}
L	Longwave radiation	kJ m^2 day^{-1}
λ_v	Latent heat of vaporization	kJ kg^{-1}
λ_f	Latent heat of fusion	kJ kg^{-1}
$LAI_{proj_{shade}}$	Shaded projected leaf area index	DIM
$LAI_{proj_{sunlit}}$	Sunlit projected leaf area index	DIM
$litter_{rain_{cap}}$	Maximum litter interception capacity	m
$livewood_{turnover}$	Rate of sapwood to heartwood turnover	%
lnc	Leaf nitrogen concentration	kg(Nleaf/m^2)
LWP	Leaf water potential	MPa
$LWP_{min.spring}$	Fully open stomata leaf water potential	MPa
$LWP_{predawn}$	Predawn leaf water potential	MPa
m	Decay rate of hydraulic conductivity with depth	DIM
M_{rad}	Radiation melt	m day^{-1}
M_T	Latent and sensible heat melt	m day^{-1}
M_V	Advective melt	m day^{-1}
mortality	Annual plant mortality rate	% yr^{-1}
$N_{dentrif}$	Denitrification rate	kgN m^{-2} day^{-1}
N_{nitrif}	Nitrification rate	kgN m^{-2} day^{-1}
N_{soil}	Soil nitrogen mass	kgN m^2
$ndep_{NO_3}$	Atm NO_3 deposition	kgN m^{-2} day^{-1}
$ndep_{NH_4}$	Atm NH_4 deposition	kgN m^{-2} day^{-1}
net_{psn}	Net daily photosynthesis	kgN m^{-2} day^{-1}
nlc	Percentage of NPP to be allocated daily	%
NH_{4conc}	Soil ammonium concentration	kgN m^{-3}
$NO3_{decay}$	Parameter: vertical distribution of N in rooting zone	DIM
$NO3_{out}$	Total export of nitrate N from patch	kgN m^{-2} day^{-1}
$NO3_{mobile}$	Proportion of soil nitrate that is mobile	%
$NO3_{surface}$	Nitrate at top of soil profile	kg m^{-2}
NO_3.soil	Available nitrate in the soil	kgN m^{-2}
$\omega_{a,b}$	Flow width between patch a and b	m
p	Decay of porosity with depth	DIM
P	Precipitation	m day^{-1}
ϕ	Porosity	%
ϕ_0	Surface porosity	%
p_a	Atmospheric pressure	Pa
PAI	Plant area index	DIM

A2. (*Continued*)

Variable	Description	Units
$PAR_{direct'}$	Incoming direct PAR radiation	kJ m^{-2} day^{-1}
$PAR_{diffuse'}$	Incoming diffuse PAR radiation	kJ m^{-2} day^{-1}
$pot_{q_{exfil}}$	Potential exfiltration rate	m day^{-1}
$ppfd_{shade}$	Shaded leaf photon flux density	μmol m^{-2} s^{-1}
$ppfd_{sunlit}$	Sunlit leaf photon flux density	μmol m^{-2} s^{-1}
psn_{actual}	Photosynthesis (with water, N limitation)	kgC m^{-2} day^{-1}
psn_{pot}	Photosynthesis (no water, N limitation)	kgC m^{-2} day^{-1}
q_{base}	Baseflow for the hillslope	m day^{-1}
q_{cap}	Capillary rise	m day^{-1}
q_{drain}	Unsaturated zone drainage	m day^{-1}
q_{infil}	Infiltration	m day^{-1}
q_{melt}	Snowmelt	m day^{-1}
q_z	Net lateral transport of water from the patch	m day^{-1}
$q(t)_{a,b}$	Saturated throughflow	m day^{-1}
R_{net}	Net radiation	kJ m^{-2} day^{-1}
R_{NO_3}	Maximum denitrification rate	kgN m^{-2} day^{-1}
ρ_{water}	Density of water	kg m^{-3}
r_w	Species specific empirical constant	DIM
ra_o	Overstory resistance	s m^{-1}
ra_u	Understory resistance	s m^{-1}
rain	Incoming precipitation	m
RT	Rain throughfall	m
s	Saturation deficit (water)	m(water)
S	Relative soil moisture content	%
S	Rooting zone soil wetness	%
$\bar{s}$	Hillslope mean saturation deficit	m
$s_{active.soil.depth}$	Soil hydrologic depth	m
S_c	Scattering coefficient	0 − 1
$S_{fc}(z)$	Relative saturation at field capacity	%
S_{litter}	Current water content	m
S_p	Sorptivity	$m/\sqrt{day}$
s_{unsat}	Soil moisture content of the unsaturation zone	m
SED	Snowpack energy deficit	°C
SED_{max}	Maximum energy deficit	°C
$\bar{s}'$	Hillslope mean saturation deficit, w capillary fringe	m
σ	Stefan–Boltzmann constant	cal cm^{-2} day^{-1} K^4
soil.N.avail	Total mineral soil N	kgN m^{-2}
soil.NH_4	Soil ammonia	kgN m^{-2}
soil.NO_3	Soil nitrate	kgN m^{-2}
soil.sminn	Mineralized soil nitrogen	kgN m^{-2}
$surf_{NO3}$	Nitrate in surface detention store	kg m^{-2}
swa	Stem wood equivalent area	DIM
Trp	Total transpiration	m day^{-1}
T_{air}	Mean daily temperature	°C
T_{avg}	Average daily temperature	°C
t_d	Precipitation duration	days
T_{day}	Mean daytime temperature	°C
T_e	Mean hillslope transmissivity	m day^{-1}
T_{max}	Maximum daily temperature	°C
$T_{max_{snow}}$	Maximum temperature at which snow can occur	°C
T_{min}	Minimum daily temperature	°C

A2. (*Continued*)

Variable	Description	Units
$T_{\min_{rain}}$	Minimum temperature at which rain can occur	°C
$T_{night_{max}}$	Night time temperature at sundown	°C
T_o	Local transmissivity	m day^{-1}
t_p	Time to ponding	days
T_{soil}	Soil temperature	°C
t_{scale}	Temperature scalar multiplier	0–1
TF	Net throughfall from canopy layers	m day^{-1}
θ	Soil moisture	%
θ_0	Initial soil moisture content	%
θ_{fc}	Field capacity	%
Θ_I	Current interception storage	m
$\Theta_{I_{max}}$	Specific rain capacity	m
$\Theta_{I'}$	Relative interception storage	m
Θ_{noon}	Solar angle at noon	deg
θ_{unsat}	Unsaturated soil moisture	%
$total_{mr}$	Total canopy maintenance respiration	kgC m^{-2} day^{-1}
Tr	Transmissivity	m day^{-1}
u^*	Wind speed	m s^{-1}
u^*	Friction velocity	m s^{-1}
u_o	Wind-speed at top of canopy	m s^{-1}
φ_{ae}	Air entry pressure	m
$\bar{w}$	Mean hillslope wetness index	DIM
w_i	Local wetness index	DIM
w_{scale}	Soil moisture scalar multiplier	0–1
z	Saturation depth	m
z_o	Overstory canopy height	m
z_{sc}	Screen height	m
z_{soil}	Soil depth	m
z_u	Understory canopy height	m
z_{zone}	Zone elevation	m
zo_0	Roughness length	m
zo_o	Understory zero plane displacement	m
zo_u	Understory roughness length	m

References

Aber, J. D., and J. M. Melillo, 1991: *Terrestrial Ecosystems*. Saunders College Publishing, 429 pp.

Ambroise, B., K. J. Beven, and J. Freer, 1996: Towards a generalisation of the topmodel concepts: Topographic indices of hydrological similarity. *Water Resour. Res.,* **32,** 2135–2145.

Band, L., 1993: Effect of land surface representation on forest water and carbon budgets. *J. Hydrol.,* **150,** 749–772.

——, D. Peterson, S. Running, J. Coughlan, R. Lammers, J. Dungan, and R. Nemani, 1991: Forest ecosystem processes at the watershed scale: Basis for distributed simulation. *Ecol. Modell.,* **56,** 171–196.

——, J. Patterson, R. Nemani, and S. Running, 1993: Forest ecosystem processes at the watershed scale: Incorporating hillslope hydrology. *Agric. For. Meteor.,* **63,** 93–126.

——, C. Tague, S. Brun, D. Tenenbaum, and R. Fernandes, 2000: Modelling watersheds as spatial object hierarchies: Structure and dynamics. *Trans. Geogr. Info. Syst.,* **4,** 181–196.

——, ——, and P. Groffman, 2001: Forest ecosystem processes at the watershed scale: Hydrological and ecological controls of nitrogen export. *Hydrol. Processes,* **15,** 2013–2028.

Baron, J. S., M. D. Hartman, T. G. F. Kittel, L. E. Band, D. S. Ojima, and R. B. Lammers, 1998: Effects of land cover, water redistribution, and temperature on ecosystem processes in the South Platte basin. *Ecol. Appl.,* **8,** 1037–1051.

Beven, K., and M. Kirkby, 1979: A physically-based variable contributing area model of basin hydrology. *Hydrol. Sci. Bull.,* **24,** 43–69.

Chen, J., P. M. Rich, S. Gower, J. Norman, and S. Plummer, 1997: Leaf area index of boreal forests: Theory, techniques, and measurements. *J. Geophys. Res.,* **102,** 29 429–29 444.

——, J. Liu, J. Cihlar, and M. Goulden, 1999: Daily canopy photosynthesis model through temporal and spatial scaling for remote sensing applications. *Ecol. Modell.,* **124,** 99–119.

Clapp, R., and G. Hornberger, 1978: Empirical equations for some soil hydraulic properties. *Water. Resour. Res.,* **14,** 601–604.

Coughlan, J., and S. Running, 1997: Regional ecosystem simulation: A general model for simulating snow accumulation and melt in mountainous terrain. *Landscape Ecol.,* **12,** 119–136.

Creed, I., and L. Band, 1998: Exploring functional similarity in the export of nitrate-n from forested catchments: A mechanistic modeling approach. *Water Resour. Res.,* **34,** 3079–3093.

——, C. Tague, R. Swanson, and R. L. Rothwell, 2000: The potential impacts of harvesting on the hydrologic dynamics of boreal watersheds. *Proc. American Geophysical Union 2000 Spring Meeting*, Washington, D. C., Amer. Geophys. Union.

Croley, T., 1989: Veritable evaporation modeling on the Laurentian Great Lakes. *Water Resour. Res.,* **25,** 781–792.

Daly, C., R. Neilson, and D. Phillips, 1994: A statistical–topographic model for mapping climatological precipitation over mountainous terrain. *J. Appl. Meteor.,* **33,** 140–157.

Dickenson, R., M. Shaikh, R. Bryant, and L. Graumlich, 1998: Interactive canopies for a climate model. *J. Climate,* **11,** 2823–2836.

Dingman, S., 1994: *Physical Hydrology.* Prentice Hall, 646 pp.

Dunne, T., and L. Leopold, 1979: *Water in Environmental Planning*. W. H. Freeman and Company, 818 pp.

Eagleson, P., 1978: Climate, soil and vegetation. 3. A simplified model of soil moisture movement in the liquid phase. *Water Resour. Res.,* **14,** 722–730.

Evans, J., and A. Jakeman, 1998: Development of a simple, catchment-scale, rainfall–evapotranspiration–runoff model. *Environ. Modell. Software,* **13,** 385–393.

Farquhar, G., and S. vonCaemmerer, 1982: Modeling photosynthetic response to environmental conditions. *Encyclopedia of Plant Physiology,* O. Lange et al., Eds., New Series, Vol. 12B, Springer-Verlag, 549–587.

Gold, A., P. Groffman, K. Addy, D. Kellog, M. Stolt, and A. Rosenblatt, 2001: Landscape attributes as controls on groundwater nitrate removal capacity of riparian zones. *J. Amer. Water Resour. Assoc.,* **37,** 1457–1464.

Green, W., and G. Ampt, 1911: Studies on soil physics. 1: The flow of air and water through soils. *J. Agric. Sci.,* **4,** 1–24.

Hartman, M., J. Baron, R. Lammers, B. Cline, and L. T. Band, 1999: Simulations of snow distribution and hydrology in a mountain basin. *Water Resour. Res.,* **35,** 1587–1603.

Heddeland, I., and D. Lettenmaier, 1995: *Hydrological Modeling of Boreal Forest Ecosystems.*

Water Resource Series, Vol. 14, Dept. of Civil Engineering, University of Washington, 38 pp.

Jarvis, P., 1976: The interpretations of the variations in leaf water potential and stomatal conductance found in canopies in the field. *Philos. Trans. Roy. Soc. London,* **B273,** 593–610.

Jones, H., 1992: *Plants and Microclimate: A Quantitative Approach to Plant Physiology.* Cambridge University Press, 452 pp.

Kelliher, F., T. Black, and D. Price, 1986: Estimating the effects of understory removal from a douglas fir forest using a two-layer canopy evapotranspiration model. *Water Resour. Res.,* **22,** 1891–1899.

Krezek, C., 2001: Climatic regulation of peak flows and their contributing source areas under natural and disturbed conditions in the carnation creek watershed, Vancouver Island, BC, Canada. M.S. thesis, University Western Ontario, Plant Science and Environmental Studies, 255 pp.

Lammers, R., and L. Band, 1990: Automating object descriptions of drainage basins. *Comput. Geosci.,* **16,** 787–810.

——, ——, and C. Tague, 1997: Scaling behaviour of watershed processes. *Scaling-Up: From Cell to Landscape,* P. van Gardingen, G. Foody, and P. Curran, Eds., Cambridge University Press, 295–317.

Landsberg, J., and R. Waring, 1997: A generalized model of forest productivity using simplified concepts of radiation-use efficiency, carbon balance and partitioning. *For. Ecol. Manage.,* **95,** 209–228.

Laramie, R., and J. Schaake Jr., 1972: Simulation of the continuous snowmelt process. Tech. Rep. 143, Ralph M. Parsons Laboratory, Massachusetts Institute of Technology, Cambridge, MA.

Laundrum, L., C. L. Tague, and J. Baron, 2002: Modeling hydrologic and biogeochemical processes in Loch Vale watershed using the regional hydroecological simulation system (rhessys). *Proc. 36th Annual Geological Society of America, South-Central Section Meeting,* Alpine, TX, Geological Society of America, South-Central Section.

Luce, C., and T. Cundy, 1994: Parameter identification for a runoff model for forest roads. *Water Resour. Res.,* **30,** 1057–1069.

Mackay, D., and L. Band, 1997: Forest ecosystem processes at the watershed scale: Dynamic coupling of distributed hydrology and canopy growth. *Hydrol. Proc.,* **11,** 1197–1217.

Manley, R., 1977: The soil moisture component of mathematical catchment simulation models. *J. Hydrol.,* **35,** 341–356.

McDonnell, J., 1990: A rationale for old water discharge through macropores in a steep humid catchment. *Water Resour. Res.,* **26,** 2821–2832.

Medlyn, B. E., and Coauthors, 2001: Stomatal conductance of forest species after long-term exposure to elevated CO_2 concentration: A synthesis. *New Phytologist,* **149,** 247–264.

Mitchell, S. W., and F. Csillag, 2000: Does pattern matter? Handling bias, uncertainty, and stability of predicted vegetation growth in Grasslands National Park, Saskatchewan. *Proc. Fourth Int. Conf. on Integrating GIS and Environmental Modeling (GIS/EM4): Problems, Prospects and Research Needs,* Banff, Canada.

Monteith, J., 1965: Evaporation and the environment. *Proceedings of the 19th Symposium of the Society for Experimental Biology,* Cambridge University Press, 205–233.

Nash, I., and I. Sutcliffe, 1970: Streamflow forecasting through conceptual models. *J. Hydrol.,* **10,** 282–290.

Norman, J., 1981: Simulation of microclimates. *Biometeorology in Integrated Pest Management,* J. Hatfield and I. J. Thomson, Eds., Academic Press, 65–99.

Oke, T., 1987: *Boundary Layer Climates*. 2d ed. University Press, 450 pp.

Parton, W., A. Mosier, D. Ojima, D. Valentine, D. Schimel, K. Weier, and A. Kulmala, 1996: Generalized model for N_2 and N_2O production from nitrification and denitrification. *Global Biogeochem. Cycles,* **10,** 401–412.

Peters, D., J. Buttle, C. Taylor, and B. LaZerte, 1995: Runoff production in a forested, shallow soil Canadian shield basin. *Water Resour. Res.,* **31,** 1291–1304.

Phillip, J., 1957: The theory of infiltration: 4. Sorptivity and algebraic infiltration equation. *Soil Sci.,* **84,** 257–264.

Quinn, P., K. Beven, P. Chevallier, and O. Planchon, 1991: The prediction of hillslope flow paths for distributed hydrological modeling using digital terrain models. *Hydrol. Proc.,* **5,** 59–79.

Refsgaard, J., and B. Storm, 1995: MIKE SHE. *Computer Models of Watershed Hydrology,* V. Singh, Ed., Water Resources Publications, 809–846.

Running, S., and J. Coughlan, 1988: A general model of forest ecosystem processes for regional applications: Hydrologic balance, canopy gas exchange and primary production processes. *Ecol. Modell.,* **42,** 125–154.

——, and E. Hunt, 1993: Generalization of a forest ecosystem process model for other biomes, BIOME-BGC and an application for global-scale models. *Scaling Physiological Processes: Leaf to Globe,* J. R. Ehleringer and C. Field, Eds., Academic Press, 141–158.

——, R. Nemani, and R. Hungerford, 1987: Extrapolation of synoptic meteorological data in mountainous terrain and its use for simulating forest evapotranspiration and photosynthesis. *Can. J. For. Res.,* **17,** 472–483.

——, ——, D. L. Peterson, L. E. Band, D. F. Potts, L. L. Pierce, and M. A. Spanner, 1989: Mapping regional forest evapotranspiration and photosynthesis by coupling satellite data with ecosystem simulation. *Ecology,* **70,** 1090–1101.

Ryan, M. G., 1991: Effects of climate change on plant respiration. *Ecol. Appl.,* **1,** 157–167.

Tague, C., and L. Band, 2001: Simulating the impact of road construction and forest harvesting on hydrologic response using rhessys. *Earth Surface Processes Landforms,* **26,** 135–151.

——, ——, P. Groffman, and K. Belt, 2000: Spatially distributed modeling of the hydrogeologic and ecologic controls on nitrogen cycling and nitrate export for a small forested watersheds. *Proc. American Geophysical Union 2000 Spring Meeting,* Washington, D. C., Amer. Geophys. Union.

Thornton, P., 1998: Regional ecosystem simulation: Combining surface and satellite based observations to study linkages between terrestrial energy and mass budgets. Ph.D. thesis, School of Forestry, University of Montana, Missoula, 200 pp.

——, S. Running, and M. White, 1997: Generating surfaces of daily meteorological variables over large regions of complex terrain. *J. Hydrol.,* **190,** 214–251.

vanGenuchten, M., and D. Nielsen, 1984: On describing and predicting the hydraulic properties of unsaturated soils. *Ann. Geophys.,* **3,** 615–628.

Vertessy, R., T. Hatton, P. O'Shaughnessy, and M. Jayasuriya, 1993: Predicting water yield from a mountain ash forest catchment using a terrain analysis based catchment model. *J. Hydrol.,* **150,** 665–700.

Walko, R., and Coauthors, 2000: Coupled atmosphere–biophysics–hydrology models for environmental modeling. *J. Appl. Meteor.,* **39,** 931–944.

Waring, R., and S. Running, 1998: *Forest Ecosystems: Analysis at Multiple Scales*. Academic Press, 370 pp.

Watson, F., R. Vertessy, and R. Grayson, 1999: Large scale modelling of forest hydrological processes and their long term effect on water yield. *Hydrol. Processes,* **13,** 689–700.

Webster, K., I. Creed, and C. Tague, 2001: Modeling n export from the Noland Divide

watershed: The importance of climate on nitrate-n production and transport. *Gordon Research Conference on Forested Catchments: Hydrological, Geochemical, and Biological Processes,* Andover, NH.

Wemple, B. C., J. Jones, and G. Grant, 1996: Channel network extension by logging roads in two basins, Western Cascades, Oregon. *Water Resour. Bull.,* **32,** 1195–1207.

White, M., P. Thornton, and S. Running, 1997: A continental phenology model for monitoring vegetation responses to interannual climatic variability. *Global Biogeochem. Cycles,* **11,** 217–234.

Wigmosta, M., L. Vail, and D. Lettenmaier, 1994: Distributed hydrology–vegetation model for complex terrain. *Water Resour. Res.,* **30,** 1665–1679.

Williams, T., and L. Flanagan, 1997: Effect of changes in water content on photosynthesis, transpiration and discrimination agains $_{13}CO_2$ and $C_{18}O_{16}O$ in pleurozium and sphagnum. *Oecologica,* **108,** 34–46.

Zheng, D., E. Hunt, and S. Running, 1993: A daily soil temperature model based on air temperature and precipitation for continental applications. *Climate Res.,* **2,** 183–191.